

We are IntechOpen, the world's leading publisher of Open Access books Built by scientists, for scientists

6,900

Open access books available

185,000

International authors and editors

200M

Downloads

Our authors are among the

154

Countries delivered to

TOP 1%

most cited scientists

12.2%

Contributors from top 500 universities



WEB OF SCIENCE™

Selection of our books indexed in the Book Citation Index
in Web of Science™ Core Collection (BKCI)

Interested in publishing with us?
Contact book.department@intechopen.com

Numbers displayed above are based on latest data collected.
For more information visit www.intechopen.com



Experiences with Anthropogenic Aerosol Spread in the Environment

Karel Klouda, Stanislav Brádka and Petr Otáhal

Additional information is available at the end of the chapter

<http://dx.doi.org/10.5772/48439>

1. Introduction

The general public is well aware of harmful effects of solid contaminants in the atmosphere. The harmful effects depend on both the size and composition and origin of the particles. Solid particles greater than 100 micrometers remain in the air only very shortly and settle as dust. Smaller particles remain in the air substantially longer and may be transported through space. Particles smaller than 5 micrometers demonstrate aerosol properties and remain suspended in the air.

The inhalation of aerosols made of micro- and nanoparticles results in their deposition in the human respiratory system. It is expected that, depending on their diameter, surface, chemical composition of the surface etc., they are subsequently transported to other terminal organs.

There are many epidemiological studies that have identified the negative effects of these particles on respiratory and cardiovascular systems in sensitive members of the population [1]. A particularly serious effect on the cardiovascular system has been identified for inhaled ultrafine (nano) particles.

The main sources of dust, micro and nanoparticles that exceed natural background levels are anthropogenic activities, e.g. heavy industry, operations that involve metalworking and woodworking, milling, grinding, general dusty operations, etc. [2]. This has also been one of the main reasons for our measurements. The first part of the chapter presents the results of pilot and orientation measurements of means of transport in Prague, of an office building in the center of Prague, the influence of a Diesel engine type on the quantity of nanoparticles released into the atmosphere, and particles released during fire, welding, the burning of entertainment pyrotechnics, and the shooting of police weapons.

The second part of the chapter presents the results of systematic and long-term measurements of the quantities and distribution of nanoparticles at the platform of the

busiest subway station in Prague, in a cabinet-maker workshop during processing of exotic woods, and in steelworks processing raw iron using the converter method.

Nonetheless, the results of the above-mentioned experiments should be viewed as results obtained at a particular time and place. The conclusions may be associated only with the specific situation. It is nearly impossible to obtain reproducible results, which is one of the main obstacles to the standardization of nanoparticle quantity in connection with their impact on human health (toxicity) and the environment.

2. Part I - Results of quantity and distribution measurements of aerosol nanoparticles at selected anthropogenic sources

2.1. The course of the experiments

2.1.1. Type experiment I – Prague subway

The measurement of nanoparticles was conducted inside a Prague subway train travelling on the C line during its regular operation with passengers and from the terminal station Letňany to the terminal station Háje and back. The measuring technology was situated in the 2nd (or the 4th) car of the train, on a seat in the outer part of the car.

2.1.2. Type experiment II – City bus

The measurement of nanoparticles was conducted in Prague in a city bus on line No. 189, travelling from the terminal station Sídliště Lhotka to the terminal station Kačerov, and after a break the bus travelled back to the station Sídliště Lhotka. The traffic level was 2-3 (i.e. partly traffic jams). The bus model was a Karosa B941 with a Liaz ML 636 engine. In the course of the measurement the occupancy rate of the bus fluctuated and reached a maximum of 60% of the bus capacity. The measuring technology was situated on a back seat.

2.1.3. Type experiment III – Car

The measurement of nanoparticles was conducted in a car that travelled essentially the same route as in experiment II and used various ventilation regimes. The car was a Skoda Octavia 1.6 with a gasoline engine, and the measuring technology was situated at the back of the car on the floor; there were 3 people travelling in the car.

2.1.4. Type experiment IV – Office building

In this case the measurement of nanoparticles was conducted in an office building in the center of Prague, situated at the corner of Dlážděná Street and the Senovážné Náměstí square. The measurements were conducted in several rooms in various locations on the building's layout, at various vertical levels, and for various types of operations.

2.1.5. *Type experiment V – Simulated fires*

The measurements of nanoparticles were conducted at simulated fires with various compositions of burning components in an open area.

Compositions of the burning pile were:

- a. 3 straw mattresses, feather blanket, bed sheets, electric cable ca. 2 m, polystyrene ca. 1 m², dry wood from pruning natural seeding greenery;
- b. 2 tires, polystyrene ca. 1 m², rubber hoses ca. 2 m, spent engine oil 10 l, Diesel oil 5 l, penetration paint 5 l, wood edgings.

The measuring technology for experiment V was situated 5 m from the fire edge. The aerosol samples were taken 0.5 m above ground level.

2.1.6. *Type experiment VI – Diesel engines*

Measurements of nanoparticles were performed for a Diesel engine and for a modern, environment-friendly Diesel engine.

- a. The measured engine type was a Z 7701 Zetor Brno, 1600 rev., stroke volume 3922 cm³, used in old tractor technology, mining engines, etc. The engine was put into operation in a testing room for combustion engines in DIMO Kamenná (Figure 1) and the measurements were performed at the outlet in front of the building. The distance of the measuring device from the outlet was 3 m.
- b. The measured engine type was a part of a FORD –TRANSIT type FDG6 with the engine type PGFA, stroke volume 2198 cm³, year of manufacture 2009. The measurements were performed with the engine running in neutral gear. The measuring device was situated 3 m and subsequently 7 m from the exhaust pipe.

2.1.7. *Type experiment VII – Entertainment pyrotechnics*

The measurements of nanoparticles were conducted at a simulated fireworks event that used various entertainment pyrotechnics available (mega cracker, fire hornet, sparklers, Bengal light, mega California, fire fountains, etc.) on a free area (street, square, etc.). The measuring technology was situated 12 m from the area where the entertainment pyrotechnics was gradually ignited.

2.1.8. *Type experiment VIII – Welding in a workshop*

The measurements of nanoparticles were conducted in a non-ventilated maintenance workshop (ca. 70 m³). The welded product was a steel T-section 25 x 350 mm, welded with electrodes E-B 121, E 7018, SF 026126. The measuring device was situated 2.5 m from the welding location.

After the welding was completed (ca. 5 min.) the workshop was left without any activities, then the coagulation and sedimentation of particles was measured.

2.1.9. Type experiment IX – Shooting products

The measurements of nanoparticles in shooting products were conducted for weapons used by the Czech Republic Police (handgun CZ 75 D COMPACT, machine gun H&K MP5 KA4, shotgun Beneli M2, revolver King Cobra) at an open shooting range under real conditions. The gun muzzle was situated 0.5 – 0.7 m from the measuring device; the sample collection point and the gun muzzle were situated at the same height (Figure 2).

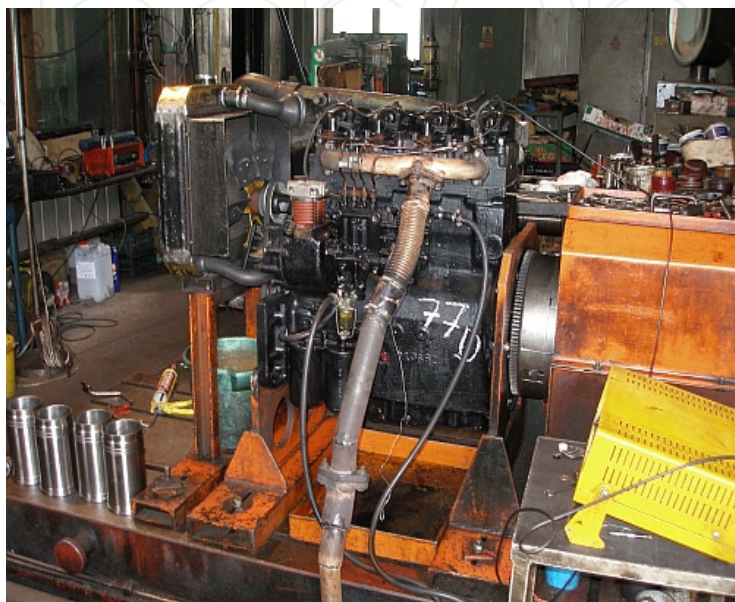


Figure 1. Tested Diesel engine type ZETOR



Figure 2. Measurement of handgun shooting

2.2. Results of the measurements and discussion

We have formulated the following conclusions from the obtained results:

- It is not possible to positively define a small increase in the quantity of nanoparticles depending on the occupancy rate of a subway car. This may be also affected by the surface locations of the stations and the subway route which may be situated close to an arterial road with busy traffic (ventilation shafts); see Figure 3 A) and 3 B).
- Passengers on the city bus line 189 were exposed to concentrations of nanoparticles higher by one order of magnitude than passengers on the subway line C (max. $36.7 \cdot 10^3$ N/cm³ in the subway, $260 \cdot 10^3$ N/cm³ on the bus). However, even in this case it is impossible to prove a positive influence of the number of passengers on the concentration of nanoparticles; the effect of traffic density and traffic composition has been considered a more likely factor.
- The effect of traffic density has been demonstrated by measurements in the car, where the quantity of particles increased in the proximity of a slip road to the Prague ring and the highway D1 (location Kačerov).
- A certain protection of persons against nanoparticles in a driving car may be ensured by the reduction of ventilation and a pollen dust filter.
- Probably the most risky particles are those with a size up to 50 nm, as they are able to penetrate a protective cell barrier. Particles of that size were primarily identified in the proximity of the Kačerov location, which is again in the proximity of the slip road to the Prague ring and the highway D1. In the subway, the most exposed section (although the levels were much lower than on the bus) was in the center of Prague near the main arterial road (stations Pankrác – Florenc).
- Quite alarming was the finding that particles smaller than 40 nm were the most abundantly ascertained by the measurement on the city bus.
- The number of nanoparticles in the working premises of the office building occupied by non-smokers and used for standard office activities was slightly lower than in the building surroundings (ca. units $\cdot 10^3$ N/cm³).
- Measurements performed in working premises on the individual floors in the building wing in the Dlážděná indicated no relationship between the quantity of nanoparticles and the floor altitude.
- An extreme increase of the number of nanoparticles was found in working premises where smoking was regular. For 3 people smoking at the same time, the number of nanoparticles increased by up to two orders of magnitude (although the levels were comparable with those on the city bus).
- Increase of the number of nanoparticles has been also demonstrated in a regular maintenance workshop.
- During fires, and during their extinguishing, the number of aerosol particles with nano dimensions strongly increased depending on the composition of the burning items (the measuring device was overloaded with fire products of mostly oil origin). The chemical composition of nanoparticles formed as burning products can be only speculated on [2].
- The increase of the overall quantity of aerosol nanoparticles for the classic Diesel engine was higher than that for the modern one, but the modern Diesel engine demonstrated an increase of nanoparticles in the dimensions that represent higher risks for human health and the environment (for comparison see Figures 4 and 5).

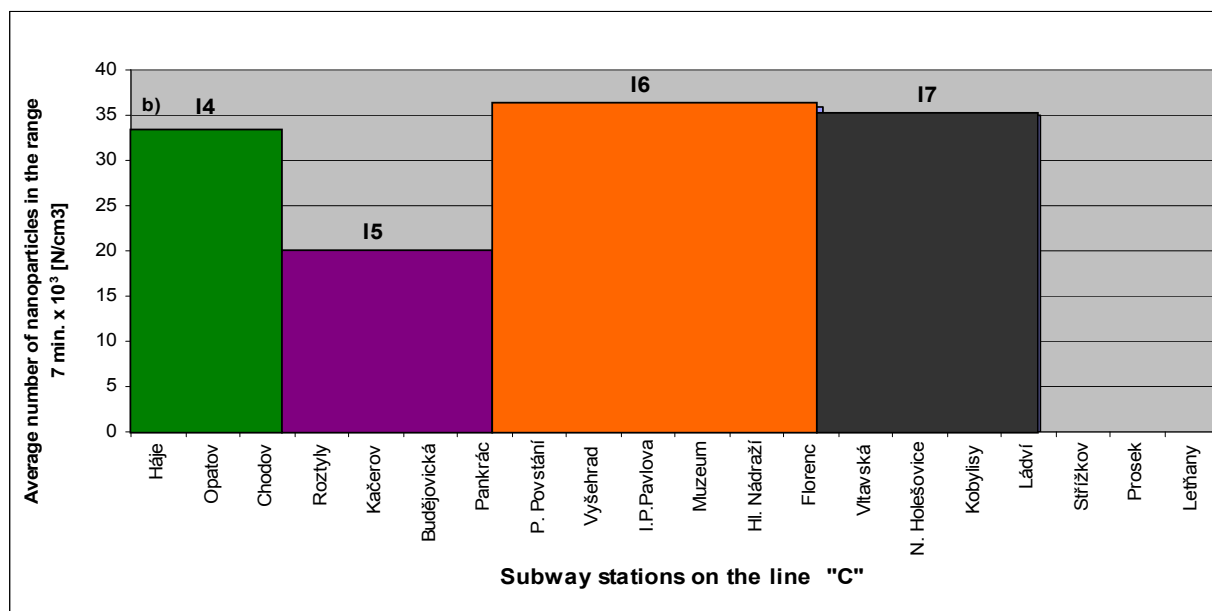


Figure 3. A) Graphic rendering of the number of nanoparticles in a subway car

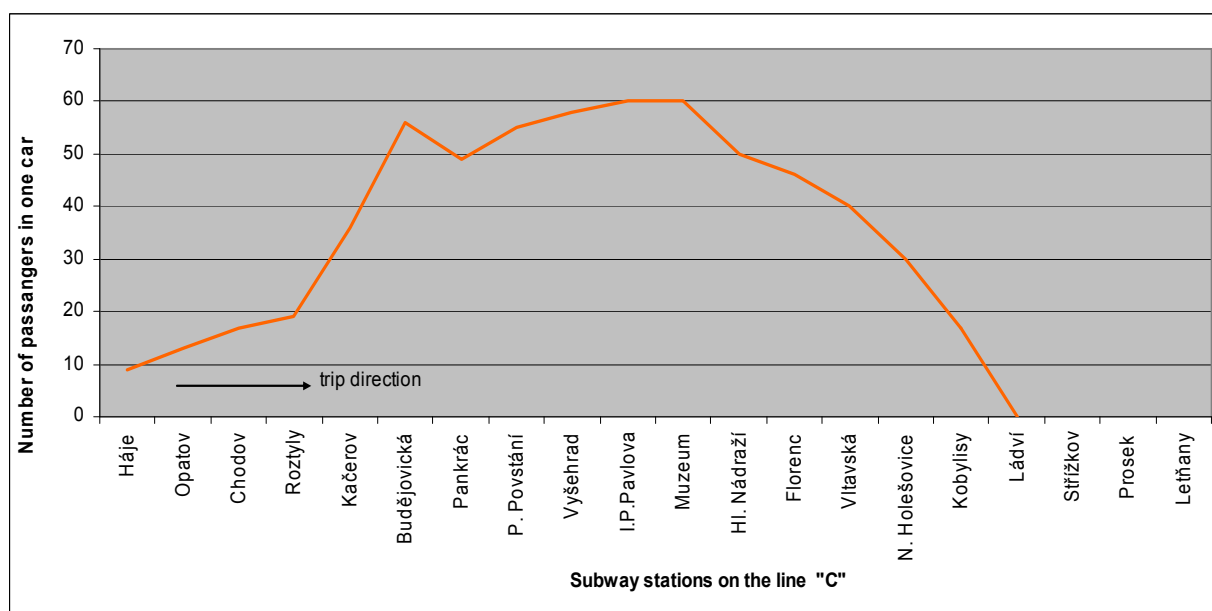


Figure 3. B) Graphic rendering of the depending on the location and number of passengers

- We have demonstrated that the concentration and size of nanoparticles change depending on the distance from their sources (see Figure 5). This is caused by dispersion and, particularly, by the coagulation of the particles (aggregation, agglomeration and adsorption of nanoparticles on microparticles, etc.).
- High-risk nanoparticles, in terms of size, have also been found for the classic engine before the engine was heated to the operating temperature (see Figure 4).
- Firefighters in action are threatened not only by particles generated by the fire and its extinguishing, but also by nanoparticles potentially generated by the firefighting technology, specifically the vehicles, Diesel aggregates, etc. (see Figure 6).

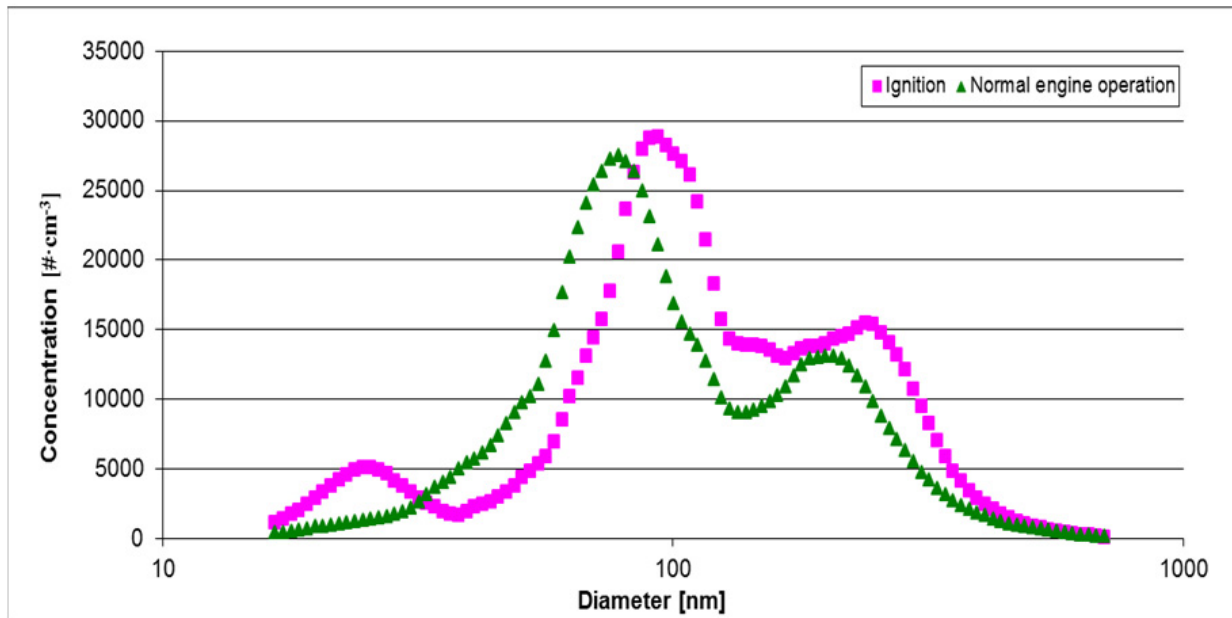


Figure 4. Distribution of particles measured at the Diesel engine made by ZETOR, exp. VI.a)

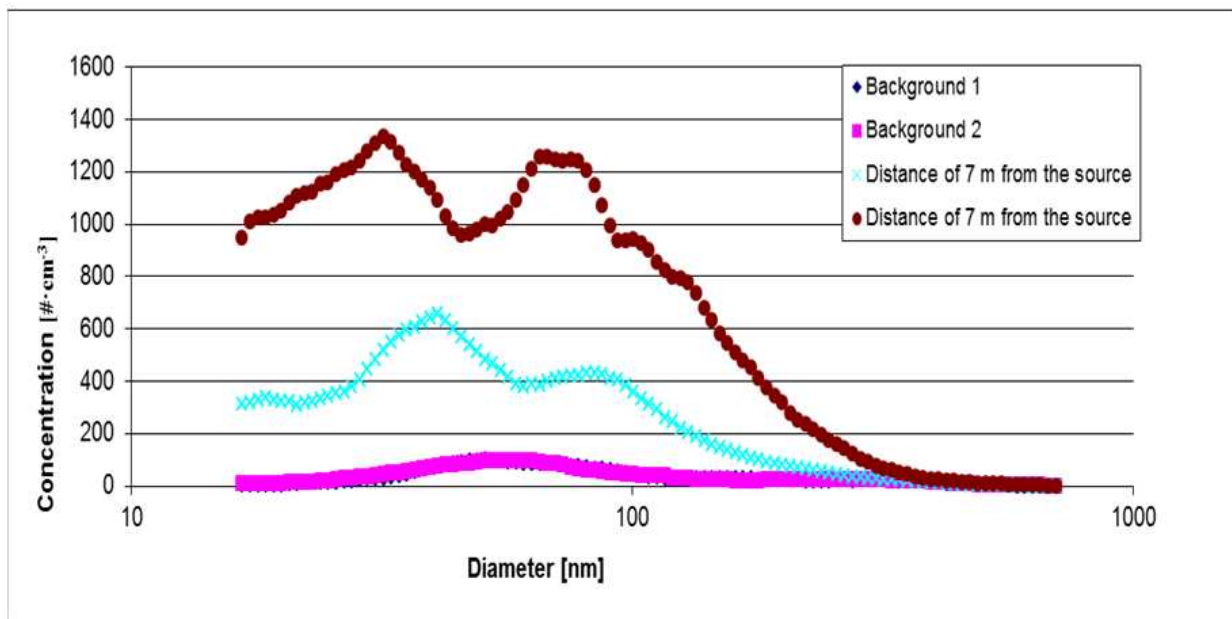


Figure 5. Distribution of aerosol particles measured at the exhaust pipe FORD TRANSIT exp. VI.b)

- The increase of nanoparticles after the ignition of entertainment pyrotechnics is two orders of magnitude higher than the background levels (see Figure 7, Table 1).
- The size of the nanoparticles from burning entertainment pyrotechnics was greater than 100 nm, while the dimensions were measured relatively far from the source. The time dependence of coagulation was also visible here; see the comparison of spectrums 2 and 3 in Figure 7.

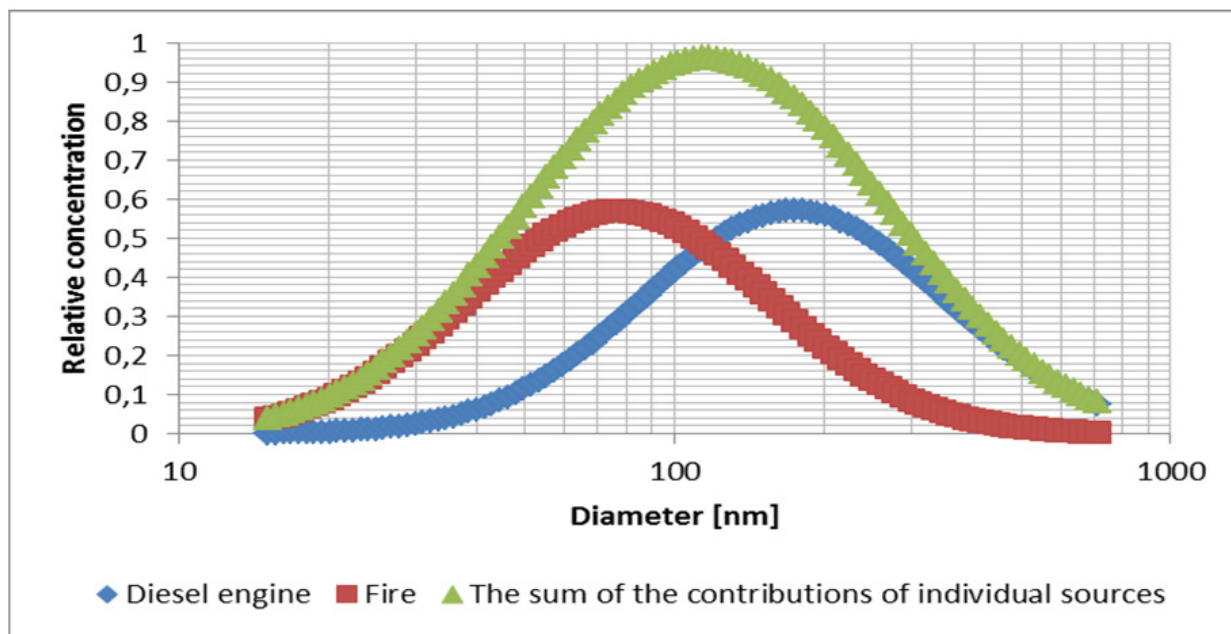


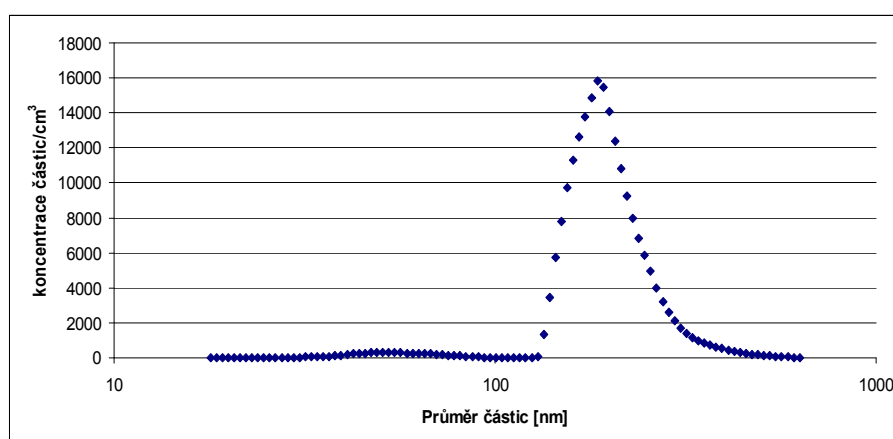
Figure 6. Distribution of particles exp. V.a

- During shooting, the overall concentration of aerosol particles per cm^2 increased, up to 200x in comparison with the initial background before shooting. Shooting products were released into the environment mainly from the weapon, the cartridge chamber, and ejected cartridge cases, and they spread in the shooting direction, to the sides and backwards.
- The highest concentration of aerosol particles after the shootings, more than double in comparison with the other weapons, was measured for the King Cobra revolver, while the spectrum had a pulsating character – see Figure 10 – and we have explained the high level of concentration of nanoparticles in after-shooting products also by the release of the products between the bullet and the muzzle.
- Dangerous nanoparticles smaller than 100 nm were generated immediately during welding, and they subsequently coagulated (see Figure 8).
- The speed of coagulation and sedimentation of particles during welding is obvious from the curve (see Figure 9, Table 2). It took essentially 3 hours before the background in the workshop dropped to the level before the welding.

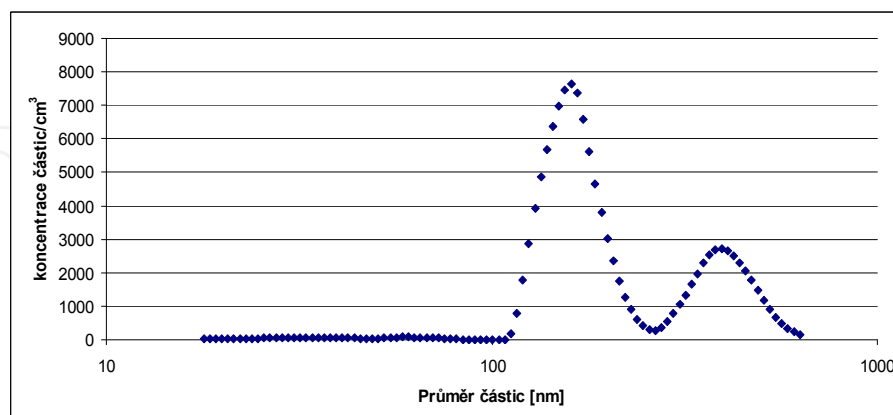
The presented results of the performed experiments have only the character of basic measurements. It is very difficult to measure the number of nanoparticles, and the results are influenced by many factors (e.g. air flow, temperature, humidity, distance from the source etc.), as explained in the introductory section. It is practically impossible to get reproducible results of measurements, and this is one of the main problems of standardization of nanoparticles in respect to their impact on human health (toxicity) and the environment [3]. For these reasons, the conclusions provided herein may be associated only with the specific situations.

	Spectrum identification	Concentration of particles/cm ³	Total weight of particles	Total volume of particles	Total surface of particles
			μg/m ³	nm ³ /cm ³	nm ² /cm ³
Background	1	1530	6.44	5.37 × 10 ⁹	1.18 × 10 ⁸
Application of pyrotechnics	2	212000	1.27 × 10 ³	1.06 × 10 ¹²	2.77 × 10 ¹⁰
Application of pyrotechnics	3	124000	1.79 × 10 ³	1.49 × 10 ¹²	2.56 × 10 ¹⁰
No pyrotechnics	4	3290	15.5	1.3 × 10 ¹⁰	2.77 × 10 ⁸

Table 1. The physical values of nanoparticles measured during entertainment pyrotechnics experiments



Spectrum No. 2 (spectrum identification see Table 1)

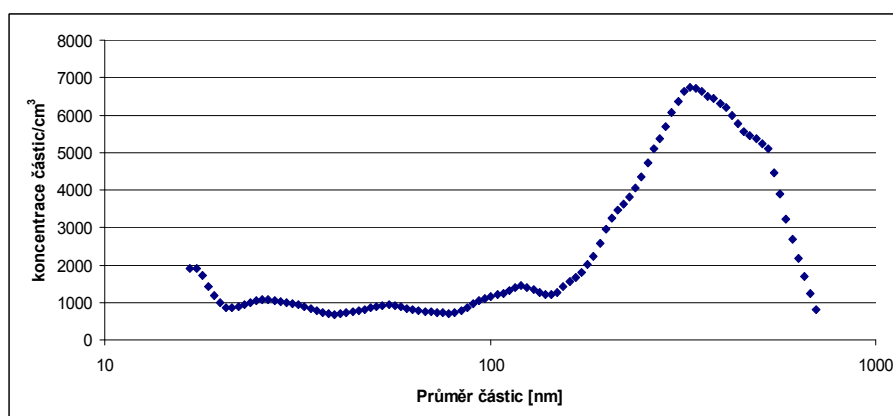


Spectrum No. 3 (spectrum identification see Table 1)

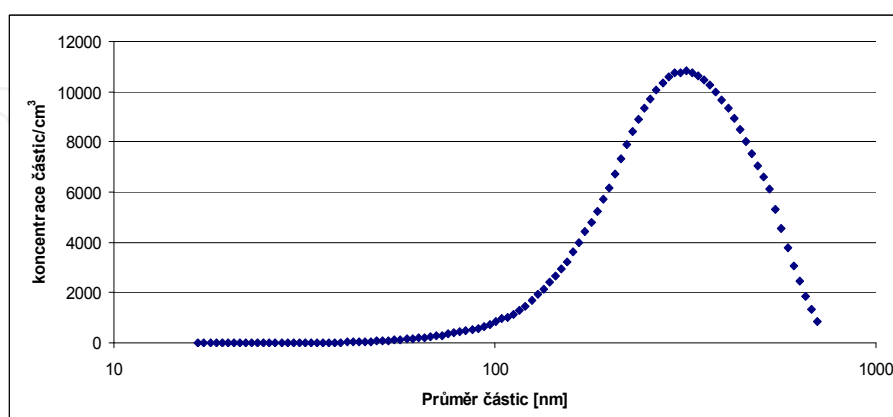
Figure 7. Spectra describing distribution of nanoparticles during entertainment pyrotechnics experiments. (Axis y: concentration of particles/cm³; axis x: diameter of particles [nm])

	Spectrum identification	Concentration of particles/cm ³	Total weight of particles μg/m ³	Total volume of particles nm ³ /cm ³	Total surface of particles nm ² /cm ³
background	1	4620	14	1.17 × 10 ¹⁰	2.9 × 10 ⁸
welding	2	256000	7240	6.03 × 10 ¹²	8.4 × 10 ¹⁰
coagulation	3	333000	9910	8.26 × 10 ¹²	1.21 × 10 ¹¹
coagulation	4	166000	5580	4.65 × 10 ¹²	6.65 × 10 ¹⁰
coagulation	5	98800	3570	2.98 × 10 ¹²	4.18 × 10 ¹⁰
coagulation	6	68900	2680	2.24 × 10 ¹²	3.08 × 10 ¹⁰

Table 2. The physical values of nanoparticles measured during welding experiments



Spectrum No. 2 (spectrum identification see Table 2)



Spectrum No. 3 (spectrum identification see Table 2)

Figure 8. Spectra describing distribution of nanoparticles during welding experiments. (Axis y: concentration of particles/cm³; axis x: diameter of particles [nm])

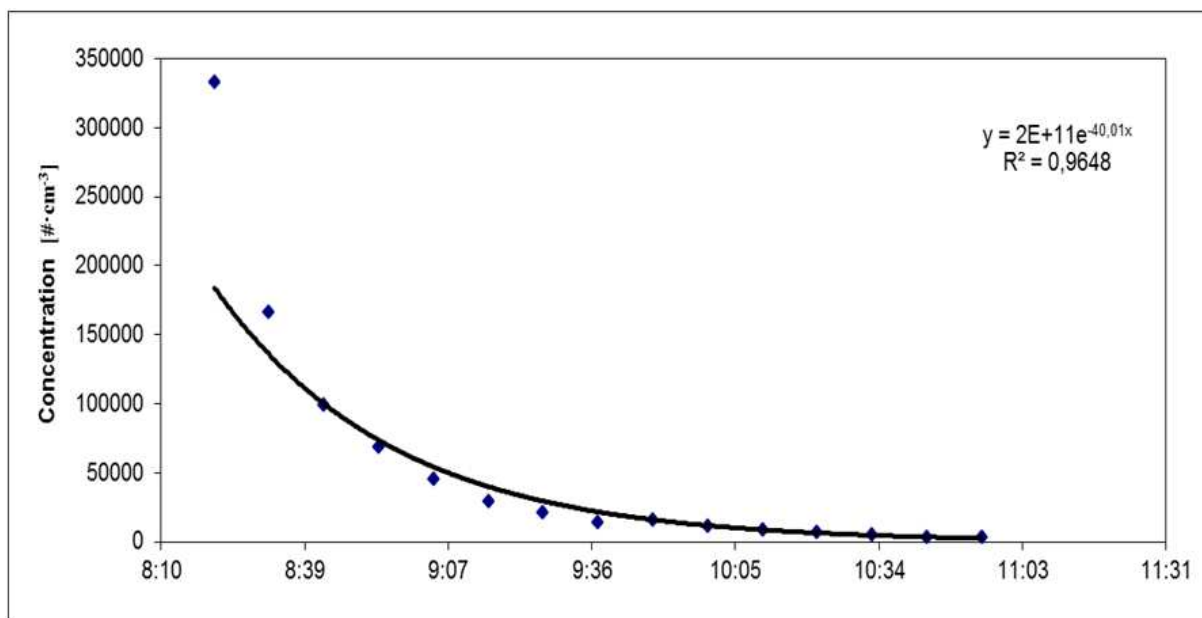


Figure 9. Rate of coagulation and deposition of nanoparticles in a workshop after welding plotted against time

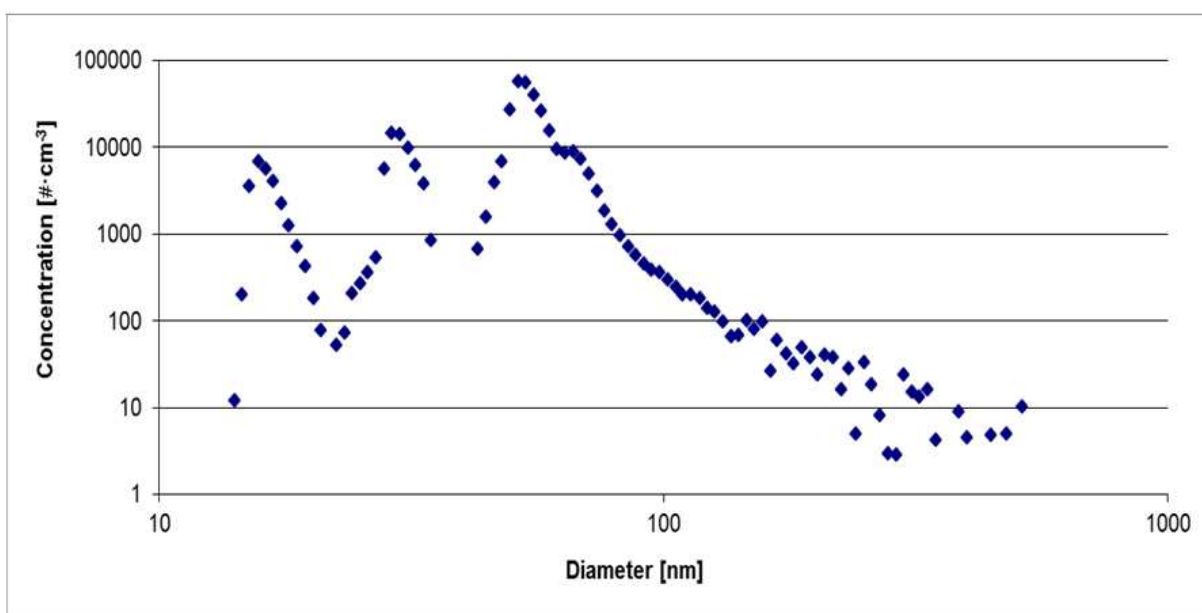


Figure 10. Revolver type weapon (King Cobra), two magazines were shot out with 6 bullets each

It was fairly alarming to find out that particles smaller than 50 nm were essentially most frequently present at a fire, extinguishing, welding, at an outlet from the modern Diesel engine and from a non-heated classic Diesel engine, and in large quantities after shooting.

Results for the Diesel engines are in agreement with the discussion and with the statement [4] that the improved combustion in modern Diesel engines extremely reduces the fraction of large particles; however, this is counterbalanced by the generation of extremely small particles: “No smoke coming from the exhaust pipe is reassuring to the eye, but the problem is in just that which cannot be seen.”

3. Part II – Results of systematic measurements

3.1. Concentration and distribution of aerosol nanoparticles in the Prague subway station Muzeum C

In March 2011 an experiment was organized with the objective of measuring the distribution of size and concentration of aerosol particles in a very busy (changing) subway station in Prague. The location of the measurements was the station Muzeum C for a period of twelve hours (the data from the meteorological station were collected from 7:15 to 0:15, the measurements were performed from 7:40 to 0:28).

The measuring technology was situated in the middle of the platform (see Figure 11). The instrument enabled measurement in the range from 14.1 to 791 nm with a sampling interval of 5 minutes.

The trains on the line C are M1 (engine power 141.5 kW). The basic data about the platform dimensions are provided in Table 3.

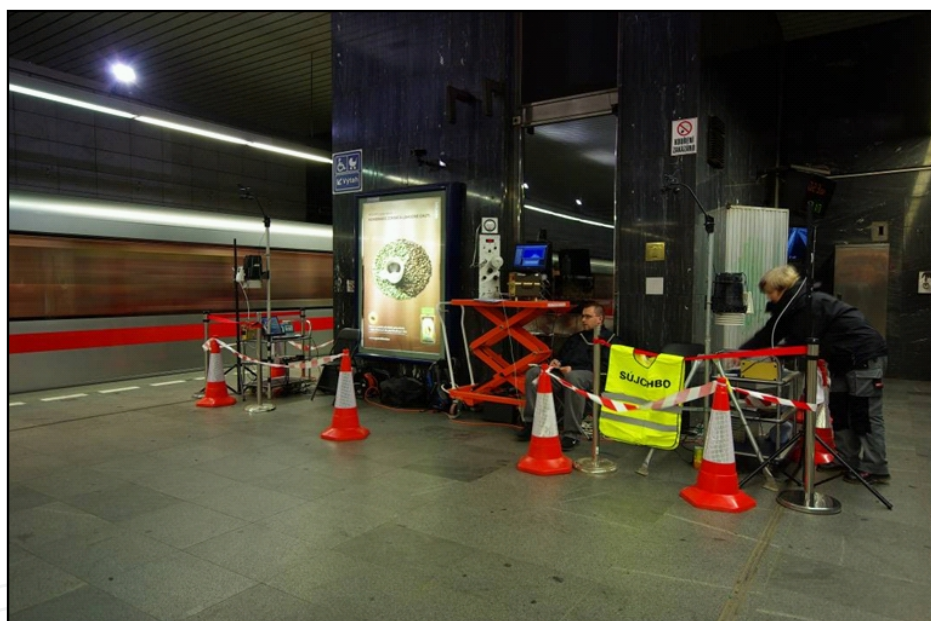


Figure 11. Location of the measuring technology on a platform of the subway station Muzeum C

Length of the station	194 m
Depth of the platform center under the ground level	10 m
Platform width	10 m
Platform height	4.3 – 5 m

Table 3. Dimensions of the subway station Muzeum C

The temperature at the platform during the measurements was 12 – 13 °C, after 21:00 hours the temperature dropped by 1.5 – 2 °C, and the air flow at the measuring device had a pulsating character – see Figure 12.

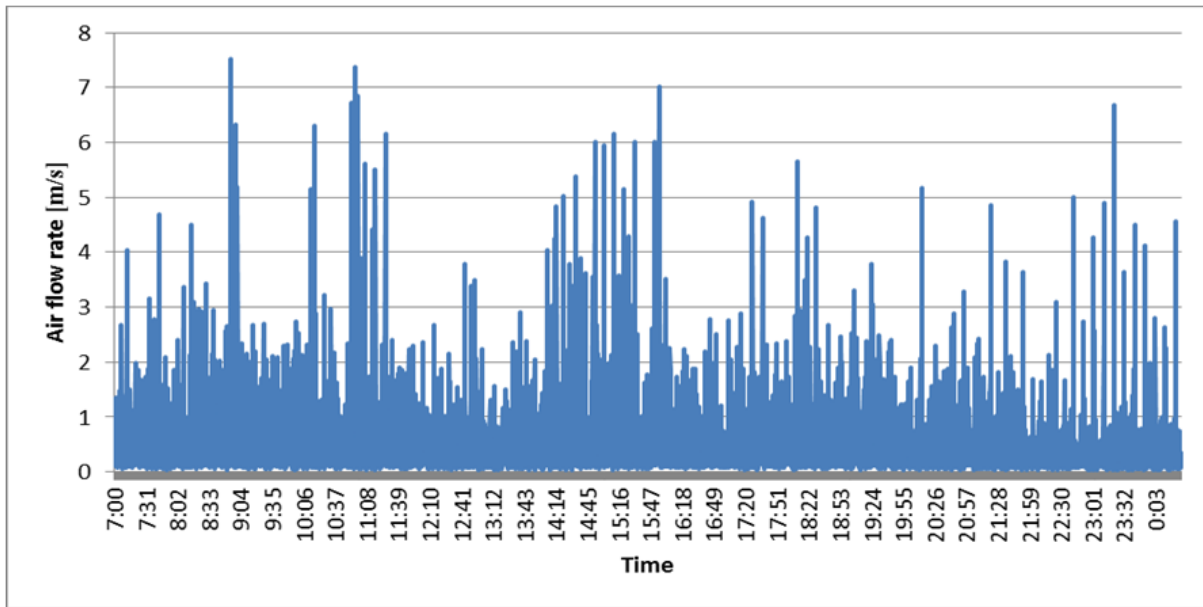


Figure 12. Air flow speed in the proximity of the measuring technology

The temperature outdoors in the morning hours was $-4\text{ }^{\circ}\text{C}$, in the afternoon $2\text{ }^{\circ}\text{C}$, and in the evening $0\text{ }^{\circ}\text{C}$. The air flow on the surface was from $2\text{ m}\cdot\text{s}^{-1}$ to $7\text{ m}\cdot\text{s}^{-1}$ (the maximum was reached between 13:00 and 14:00 hours).

3.2. Results of the measurements and discussion

The basic results of measurements of the overall concentration of aerosol particles during subway operation are shown in the diagram in Figure 13. The diagram of the concentrations of aerosol particles is completed with the intervals of subway trains passing through the station.

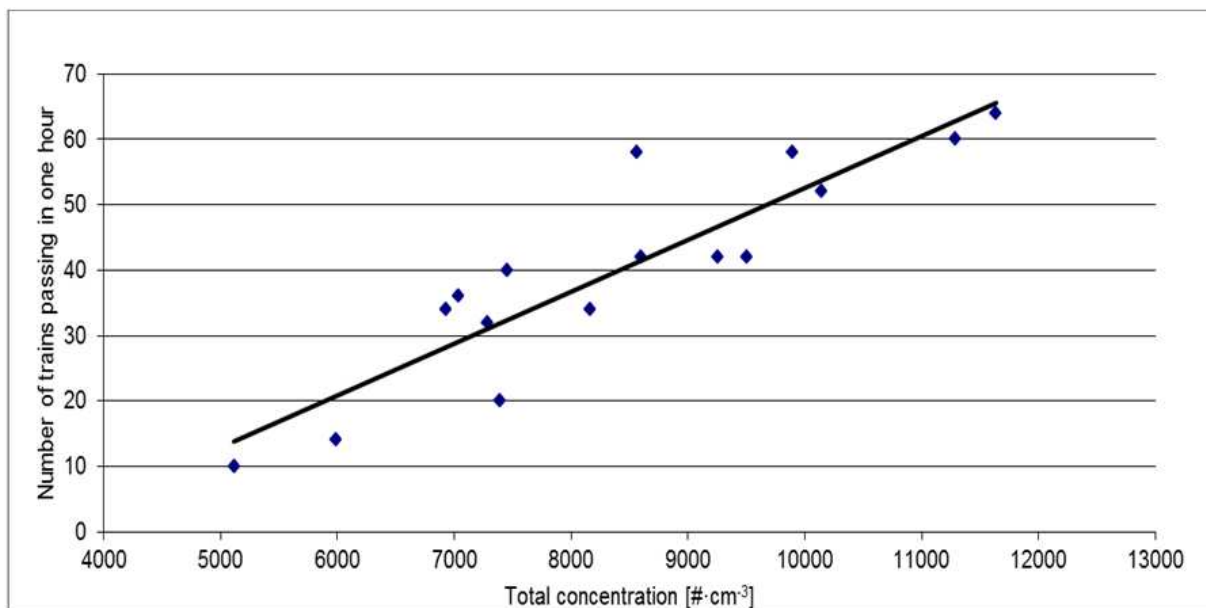


Figure 13. Overall concentration of aerosol particles during the subway operation

The diagram shown above indicates that the concentration of aerosol particles in the subway station is significantly affected by the frequency of trains passing through the station.

This fact has been confirmed by the following Figure 14, which presents a graphic rendering of the dependence of the overall concentration of aerosol particles on the number of trains passing through the subway station in both directions per hour. In theory, the diagram suggests that if there were no trains passing through the station the overall concentration of aerosols would be ca. 3400 particles per cm^3 .

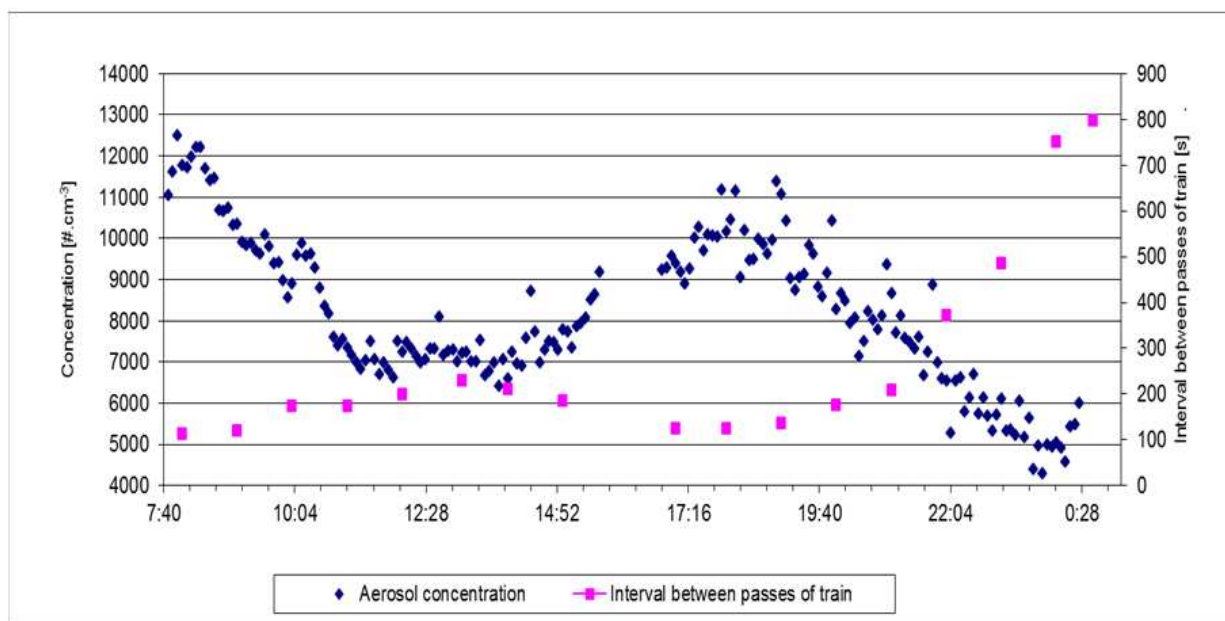


Figure 14. Comparison of the overall concentration of particles with the number of passing trains

The summary of average concentrations of aerosol particles for the monitored period is shown in Table 4. As a curiosity, we have provided also the measured concentration of aerosol particles in the environment during passage of a servicing Diesel locomotive MUV – 72 (engine TATRA T 928 – 2 with engine power 130 kW) after the passenger traffic in the station was closed.

	N.cm^{-3}	Standard deviation
Overall average (without the locomotive)	8200	± 1800
Morning rush hour ($7^{45} - 9^{45}$)	10800	± 950
Morning low ($11^{30} - 14^{30}$)	7200	± 420
Afternoon rush hours ($17^{30} - 19^{30}$)	9980	± 700
Night low ($22^{00} - 0^{30}$)	5520	± 600
Maximum during the passage of the servicing locomotive	35500	-

Table 4. Average concentrations of aerosol particles during the monitored period

Figures 15 and 16 are graphic renderings of distribution of the particles during the morning and afternoon rush hours and during the traffic lows.

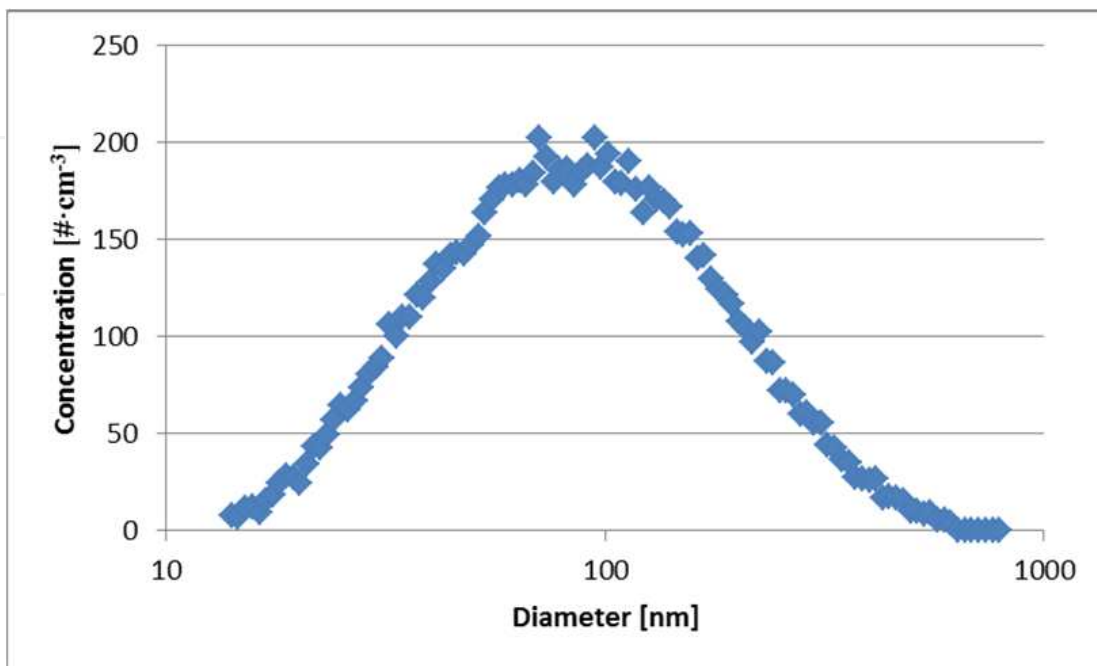


Figure 15. Distribution of particles during the morning and afternoon rush hours

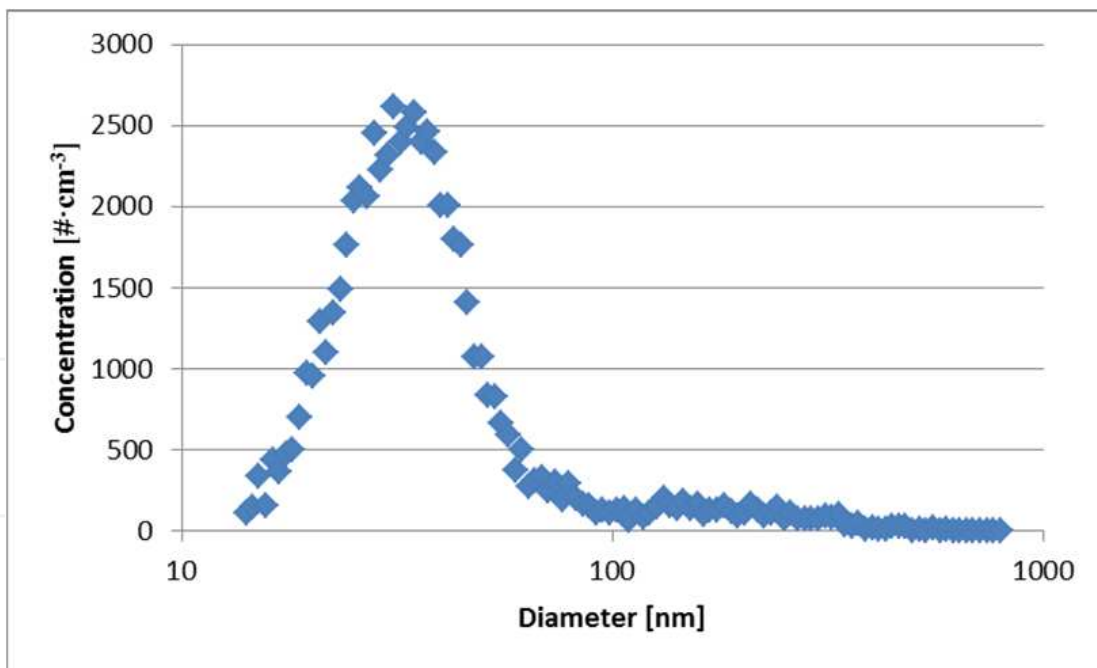


Figure 16. Distribution of particles during the morning low

Figure 17 is a graphic rendering of the distribution of particles during the passage of the servicing locomotive that passed through the station after it was closed for passenger traffic. The diagram indicates a distribution shift to smaller, i.e. more dangerous dimensions of the particles.

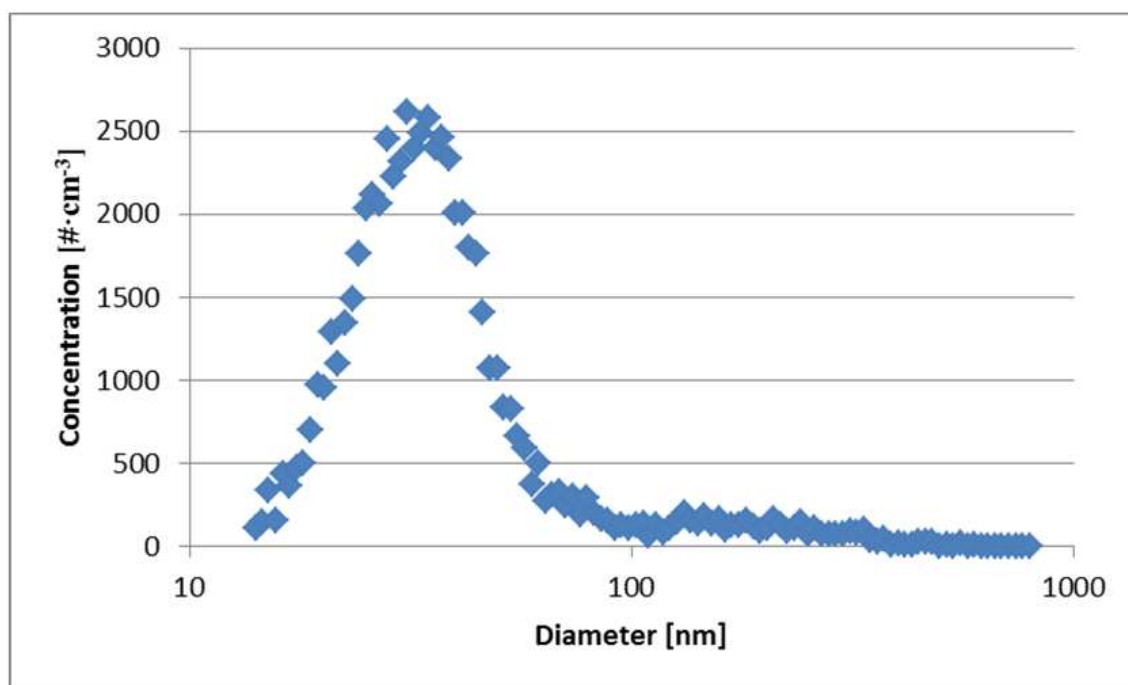


Figure 17. Distribution of particles during the passage of the servicing locomotive

What are the supposed sources of nanoparticles on the subway station platform?

- a. Supply of the outdoor air via a vent shaft (see Figure 18) into the tunnel premises in the platform proximity: In winter the ventilation air is supplied into the subway from the ground level into the tunnel premises via a vent shaft. In this case the vent shaft is situated in a very close proximity to a busy road (Prague arterial road), where the level of traffic is a “slow moving traffic jam”. The traffic on the arterial road probably influences the quantity of nanoparticles on the subway platform.
- b. Release of previously deposited nanoparticles from the tunnel premises: The increased concentration of nanoparticles is probably also influenced by pressure waves caused by passing trains in the narrowed premises of the tunnels. These may be e.g. nanoparticles generated by wear of the tunnel lining (usually reinforced concrete), wear of the rails, cross-ties, subbase and by technical operations (servicing technology).
- c. Braking of the trains: Another factor that may influence the measured quantity of nanoparticles is braking of the trains. The weight of a subway train is ca. 130 t and it brakes for several seconds. This braking results in the wear of wheels, brakes, rails, etc.
- d. Influence of passengers: During the experiment we attempted to limit this influence to the maximum extent by placing the measuring technology at the end of the platform, but we still anticipate that the measured values might have been influenced by the changing numbers of persons in the station.

We anticipate that the mostly tunnel character of the subway line is the source of aerosol nanoparticles of various origin. Their spread (release) is probably caused by pressure and impulse waves created by the running subway trains.



Figure 18. The subway vent shaft structure on the ground level near the busy road

This assumption has been confirmed by a comparison of the quantity of measured nanoparticles inside a train car on the subway platform on the line C with the quantity measured in a subway train car during its trip on the line C (see part I). The concentration of nanoparticles in the travelling train car was higher than at the same place measured on the platform. This is probably caused by the ventilation system of the cars which takes in the air from the tunnel premises, plus by the higher concentration of passengers per area unit.

3.3. Aerosol and dust particles generated during processing of selected exotic woods

The objective of the measurements was to measure quantities and distribution of aerosol micro and nanoparticles generated by individual technological steps during processing of various types of tropic woods used on the market in the Czech Republic. At the same time, we also focused on the microstructure of the wood dust in the deposits and difference in the

chemical composition of the individual woods; this may play a negative role after they get into the respiratory system or into contact with skin or eye mucosa. We focused on tropical woods due their wide variety and the dramatic increase of their import to the processing market in the Czech Republic.

Wood processing generates wood dust which may, depending on the size of the particles, form an aerosol or settle directly. The wood dust contains chemical substances that form the wood (polysaccharides, such as cellulose and hemicellulose, aromatic substances, such as lignin and tannins, resin terpenes, lipids, nitrogenous substances, inorganic substances etc.) depending on the wood condition, while it is impossible to exclude the presence of biological organisms, fungi, mildews or bacteria [5].

A negative effect of the wood dust on the human organism may occur in case of contact with skin or eye mucosa or inhalation by the respiratory tract. There is a general rule that the with decreasing size of the particles their respirability increases as well as their ability to bind with other substances (by sorption or condensation). Dusts from biologically highly aggressive woods may cause dermatitis, respiratory diseases, allergic respiratory problems (asthma) and carcinogenic effects (adenocarcinoma of nasal cavity and paranasal cavity). The chemical composition of wood opens a number of possibilities in contact with the biological system [6].

The measurements were conducted in the course of full operation in a production hall (area 700 m², volume 3 500 m³) equipped with a state-of-the art filter and extraction system made by Cipres Filtr with the power output 37 kW, with a box filter CARM situated outside the hall. Despite this after a time the overall concentration of nanoparticles in the production hall increased to 4–5 × 10⁵ N/cm³. The difference from the initial level before the shift beginning is shown in the diagram in Figure 19.

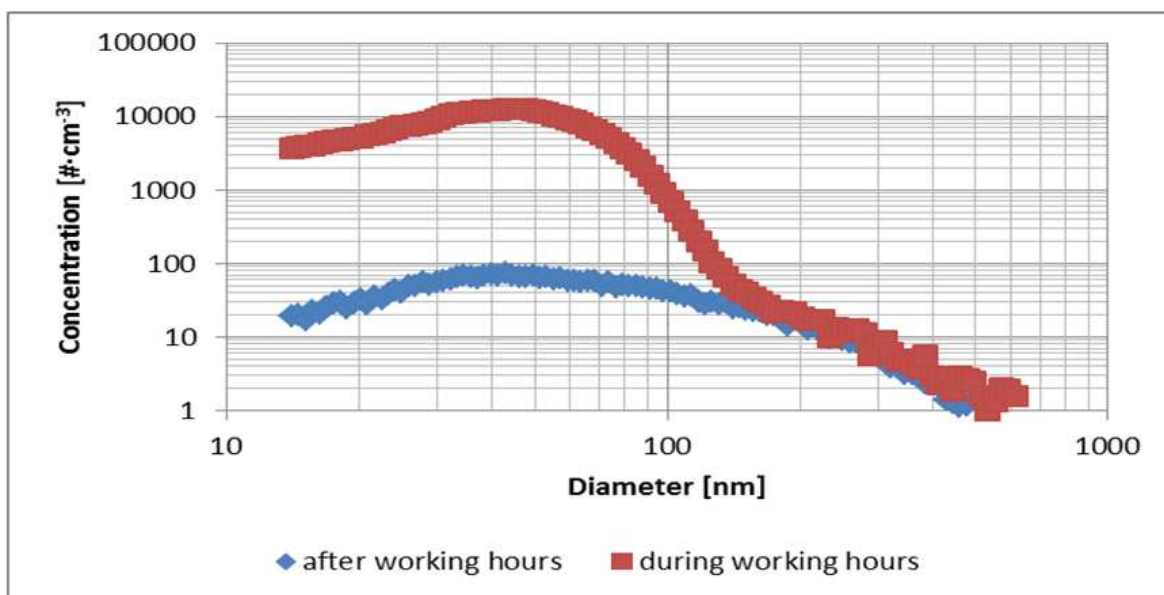


Figure 19. Comparison of the distribution of aerosol particles in the production hall during the operation and before the beginning of the operation

This has caused problems with identification of the technological process that generates the highest quantity of micro and nano aerosols. Despite those difficulties, we have identified the operation of the belt grinding machine as the main source of pollution in the production hall. The next experiment was conducted during the night, only with the technological operation of wood surface grinding with a grinding belt (belt grinding machine HOUFEK, PBH 300 B BASSEL, belt speed 17 m/s, grinding belt roughness AA 80, AA 100).

The temperature and humidity in the production hall: 24-25°C, 55%.

Tested woods: Ipé, Jatoba, Massaranduba, Merbau, Bangkirai, Faveira, Garapa, Teak, Bilinga.

The basic information on the tested tropic woods and on their processability and toxicity reported in literature is provided in Table 5.

Trade name of wood species	Latin name of wood species	Occurrence	Note about the wood processing [6]	Note about the toxicity [6]
Ipé	<i>Tabebuia spp.</i>	Central and South America	Planing is difficult, high-performance machinery is needed, very strong material, highly durable	Sawdust and grinding dust contain lapachol – as the dyestuff, it is irritating, may damage mucosa and cause dermal problems
Jatoba	<i>Hymenaea spp.</i>	Central and South America	Sawing – high-performance machinery is needed	Risk of mucosa and skin damage
Massaranduba	<i>Manilkara spp.</i>	South and tropical America (Brazil, Columbia)	Sawing – high-performance machinery is needed	Sawdust may be irritant, wood dust may irritate mucosa and skin
Merbau	<i>Intsia bakerie Prain</i>	Southeast Asia (Indonesia, Malaysia)	dulls the tools, difficult processing – special tools are needed	Chemical reaction with iron
Balau, Yellow (Bangkirai)	<i>Shorea argentea</i>	Southeast Asia (Malaysia, Indonesia)	Difficult processing	Not detected
Faveira	<i>Porkia spp.</i>	Tropical South America (Brazil, Columbia)	Easy sawing, processing without difficulties	Poor resistance against fungi and insects
Garapa*	<i>Apuleia Leiocarpa</i>	South America (Brazil)	Not detected	Allergenic and toxic
Teak	<i>Tectona Grandis</i>	Southeast Asia (Indonesia, Burma, Laos)	Sawing not completely easy, makes the tools blunt	Wood dust irritates skin, contains oily resins, resists decay
Bilinga (Opepe)	<i>Vaucle and Diderrichii</i>	West Africa (Sierra Leone, Nigeria, Cameroon)	Sawing requires high-performance machinery	Resistant against termites, the bark contains alkaloid

Table 5. Basic data about the tested woods

The layout of the measuring technology is shown in Figure 20.



Figure 20. Layout of the measuring technology in respect to the belt grinding machine:

- a. measurements of FIT factors,
- b. measurements of distribution of aerosol particles (micro),
- c. measurements of distribution of aerosol (nano) particles, d) cascade impactor.

In addition to the measurements of quantities and distribution of nano and micro aerosol particles we also measured the FIT factor to verify protective capacities of the respirators and collected samples of sedimented dust (sawdust).

3.4. Results and discussion

3.4.1. Determination of quantities of grinded-off wood

The weighted samples (mostly with the same area sizes) of exotic woods were grinded under the same conditions for 5 minutes on a belt grinding machine (see Figure 20). After the grinding was completed, the samples were weighed and the weight loss was converted into the area per 1 cm². The results shown in Table 6 indicate that the highest weight loss was found for the wood Garapa, while the values for Massaranduba, Ipé and Teak were comparable. The wood most durable against the employed grinding method was Merbau. We also compared the quantities of ground-off wood material depending on the grit size of the grinding belts and we found out that finer surface resulted in a higher weight of the ground-off material by up to 20-25% .

Wood (wood species)	Ground area (cm ²)	Ground-off quantity (g)	Ground-off quantity per cm ² (g)
Massaranduba	371	246	0.66
Ipé	371	261	0.70
Garapa	371	308	0.83
Teak	331	266	0.80
Bilinga	466	182	0.39
Jatoba	371	167	0.45
Faveira	371	157	0.42
Bangkirai	308	195	0.63
Merbau	371	78	0.21

Table 6. Determination of quantities of ground-off woods

3.4.2. Distribution of nanoparticles released during grinding of exotic woods

Examples of measured values of concentrations and distributions of aerosol particles in the range 15 – 750 nm generated by grinding of exotic woods after subtraction of the background are shown in the Figure 21.

The comparison of the above-presented diagrams of the distribution of nanoparticles in the range 7 – 100 nm has shown a detailed distribution of aerosol particles of the Ipé, Jatoba and Massaranduba woods (that belong to the category of harder materials), with the maximum at ca. 40 nm, while for the Merbau, Bangkirai and Faveira woods the maximum value shifted towards lower values.

The diagrams presented below (Figures 22 and 23) document that if we replace the grinding belt with a finer one the quantity of nanoparticles released into the atmosphere will increase, and the sizes of the particles will shift to lower values.

3.4.3. Analysis of sedimented dust:

The collected samples of sedimented dust after the wood grinding were subject to IR analysis, a microscopic study of the wood material and their thermal stability. The IR analysis sought to find a certain correlation between characteristic vibrations that may be related to the toxicity of the wood dust. The achieved microstructure of the dust was expected to provide information about the level of degradation of the wood structure by mechanical means (grinding). The thermal stability of the sedimented dust was expected to indicate the fire risks to be expected for the individual woods, while those results will be published separately.

Infrared spectroscopy is one of the few non-destructive methods for investigating the chemistry and physics of wood. Gradually, absorption bands with wave numbers have been

defined that characterize the dominant building elements of the woods, such as cellulose, hemicellulose and lignin. We have also used the FT-IR (Fourier Transform Infrared) technology to measure infrared spectrums of the collected samples of sedimented dusts. Based on the published spectrums of similar woods and catalogue values of vibrations for the specific bonds and groups [7-10], we have made assignments to the individual absorption bands. As an example, we have made assignments to the measured values of the Massaranduba wood spectrum; see Table 7 and Figure 24.

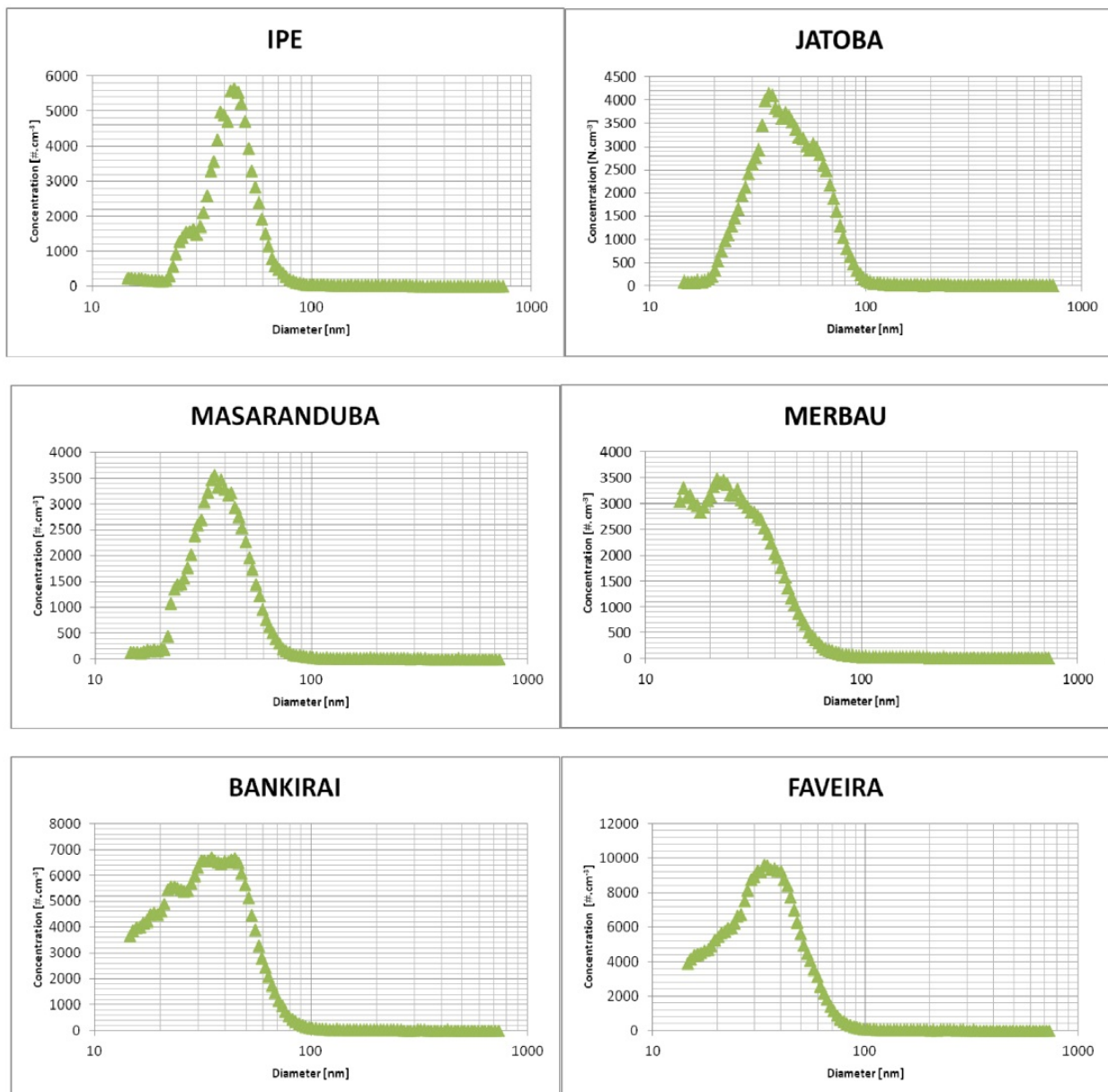


Figure 21. Distribution of aerosol particles of the woods Ipé, Jatoba, Massaranduba, Merbau, Bangkirai and Faveira, released during their grinding

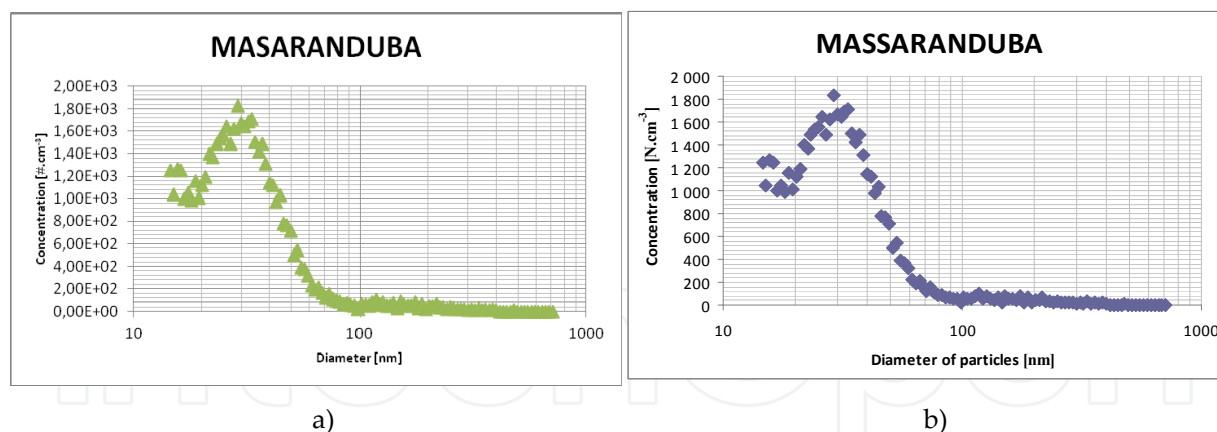


Figure 22. Distribution of aerosol particles of the Massaranduba wood a) grain size 80, b) grain size 100 (Axis y: concentration of particles/cm³; axis x: diameter of particles [nm])

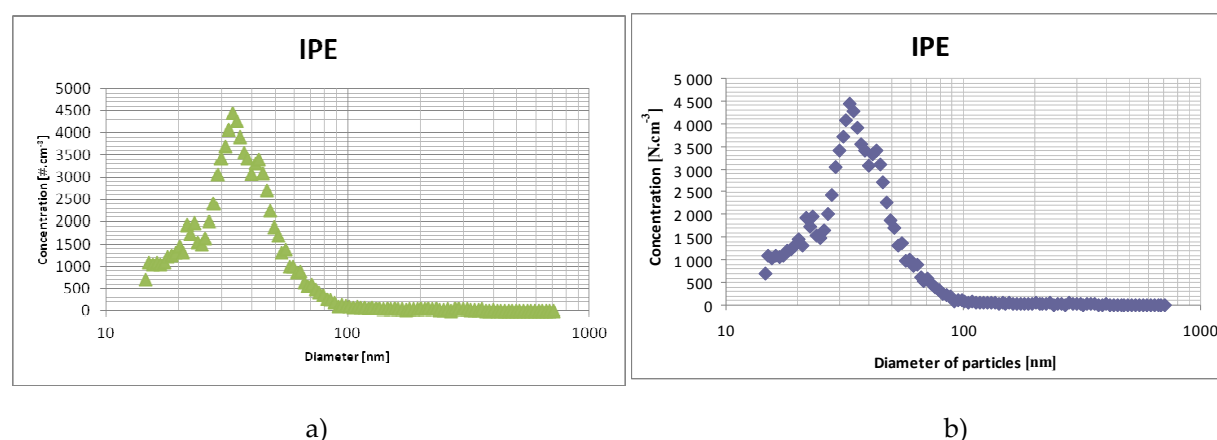


Figure 23. Distribution of aerosol particles of the Ipé wood a) grain size 80, b) grain size 100

Vibrations (cm ⁻¹)	Assignment of the functional group or skeleton
3343	O-H valence bond
2921	C-H valence bond in methyl group
1731	C=O ketone and in ester group
1593	Aromatic skeleton, valence bond C=O
1504	Aromatic skeleton, valence bond C=O
1454	C-H deformation asymmetric -CH ₃ and -CH ₂ -
1422	Vibration in the aromatic skeleton by combination with the deformation vibration in the C-H plane
1368	C-H deformation vibration in cellulose and hemicelluloses
1317	C-H vibration in cellulose and C-O vibration in syringyl derivatives
1232	Syringyl ^{a)} skeleton and bond vibration C= in lignin and xylan ^{b)}
1155	C-O-C vibration in cellulose and hemicelluloses
1023	Aromatic C-H deformation in the plane, C-OH, C-O deformation
894	Glycoside bonds
814	Planar vibration of the mannose ring

Table 7. Assignment of the wave numbers of absorption belts to specific groups or skeleton of the Massaranduba wood material. ^{a)} As a part of lignin, ^{b)} As a part of hemicellulose

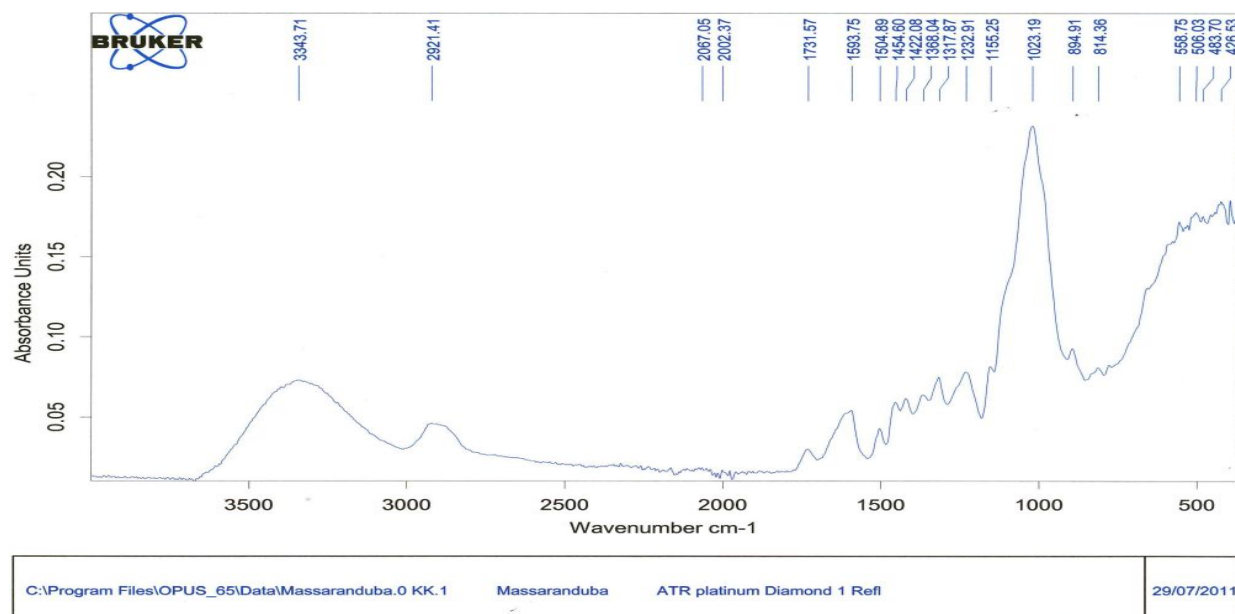


Figure 24. IR Spectrum of sedimented dust from Massaranduba wood

The comparison of the measured spectrums has shown a relative identity, particularly outside the fingerprint area of the molecule.

The variance in the wave number of C-OH vibrations is 15 cm^{-1} between the individual woods (the highest wave number 3350 cm^{-1} is for Ipé and Jatoba, the lowest is 3335 cm^{-1} for Bankirai). The variance of the valence bond vibration C-H is 72 cm^{-1} (the highest wave number is 2921 cm^{-1} for Massaranduba, the lowest is 2849 cm^{-1} for Bangkirai). The vibration shifts are probably caused by intermolecular hydrogen bonds that affect the wood density.

In the molecule fingerprint area, we focused on the identification of characteristic vibrations for various lignin skeletons and chinoid bonds (lapachol). The differences between the spectrums of the individual woods were demonstrated by absorbance values. Before the microscopic examination of the samples of sedimented dust (we will hereinafter use the term sawdust to refer to its method of origin) we described some of its external macroscopic properties and they were later confirmed at microscopic magnification by the factor of 40; they may be briefly described as follows:

- Ipé: fine sawdust with minimum dustiness
- Jatoba: sawdust of the same size as Ipé but, unlike Ipé, with significant dustiness
- Massaranduba: coarse sawdust with a structure similar to oak
- Merbau: the finest sawdust structure, with the highest dustiness
- Bangkirai: medium sawdust with a significant representation of finer particles
- Faveira: similar structure and distribution of fractions as Bangkirai
- Garapa: fine sawdust with medium dustiness and good powderiness
- Teak: sawdust with coarse structure and minimum dustiness, caused by cohesiveness or aggregation of sawdust
- Bilinga: coarse structure of sawdust with medium values of dustiness and powderiness

A summary overview of identifiable macroscopic properties is shown in Table 8

	Dustiness	Inherent cohesiveness	Powderiness	Size of particles	Structure
Ipé	+	++	+	++	Coarse
Jatoba	++	+	++	++	Coarse
Massaranduba	++	+++	++	+++	Coarse
Merbau	+++	+	+++	+	Fine
Bangkirai	+	++	++	++	Medium coarse
Faveira	+	+++	+	++	Medium fine
Garapa	++	+	++	+	Coarse
Teak	+	+++	+	+++	Coarse
Bilinga	++	++	++	++	Coarse

Table 8. Description of macroscopic properties of sedimented particles

We were interested in the shape of the particles, which will probably play a role in their fixation in the respiratory tract, so we made microscopic pictures. As an example shown below, we have provided microscopic pictures magnified 200 times, while the line segment on the pictures represents 100 micrometers; see Figure 25.

Other risks of nano-, micro- and dust particles are physicochemical, i.e. risk of fire, explosion, uncontrolled and undesired reaction. For this reason, the samples of sedimented dust were subject to thermal gravimetric analysis. For all samples of sedimented dust generated by coarse grinding, the thermal decomposition resulted in two separate exothermic processes T_1 in the range 279-333 °C (the lowest for Merbau) and T_2 in the range 402 -437 °C (the lowest for Garapa). After summarizing thermal processes during thermal decomposition of dusts of our woods, the highest thermal effects were found for the woods Jatoba (5904 kJ/kg) and Garapa (5506 kJ/kg), while the lowest value was found for the wood Teak (2210 kJ/kg).

Another finding with a safety impact was that if we use finer grains for the grinding of some woods, e.g. Massaranduba, the exothermic effect is much less significant – see the diagrams in Figure 26.

We can thus conclude that, despite a modern extraction system that was installed in the workshop, the content of aerosol nanoparticles was two orders of magnitude higher than before the production works started, and the concentrations of dust particles in the immediate proximity of the grinder were several times higher than values permitted by Czech legislation. The sizes of aerosol nanoparticles, based on the determined distribution, mean that they can pass through protective barriers of the respiratory system up to the alveoli. Here the question remains on the role played in the toxicity by the concentration, chemical composition, surface and shape of the nanoparticles.

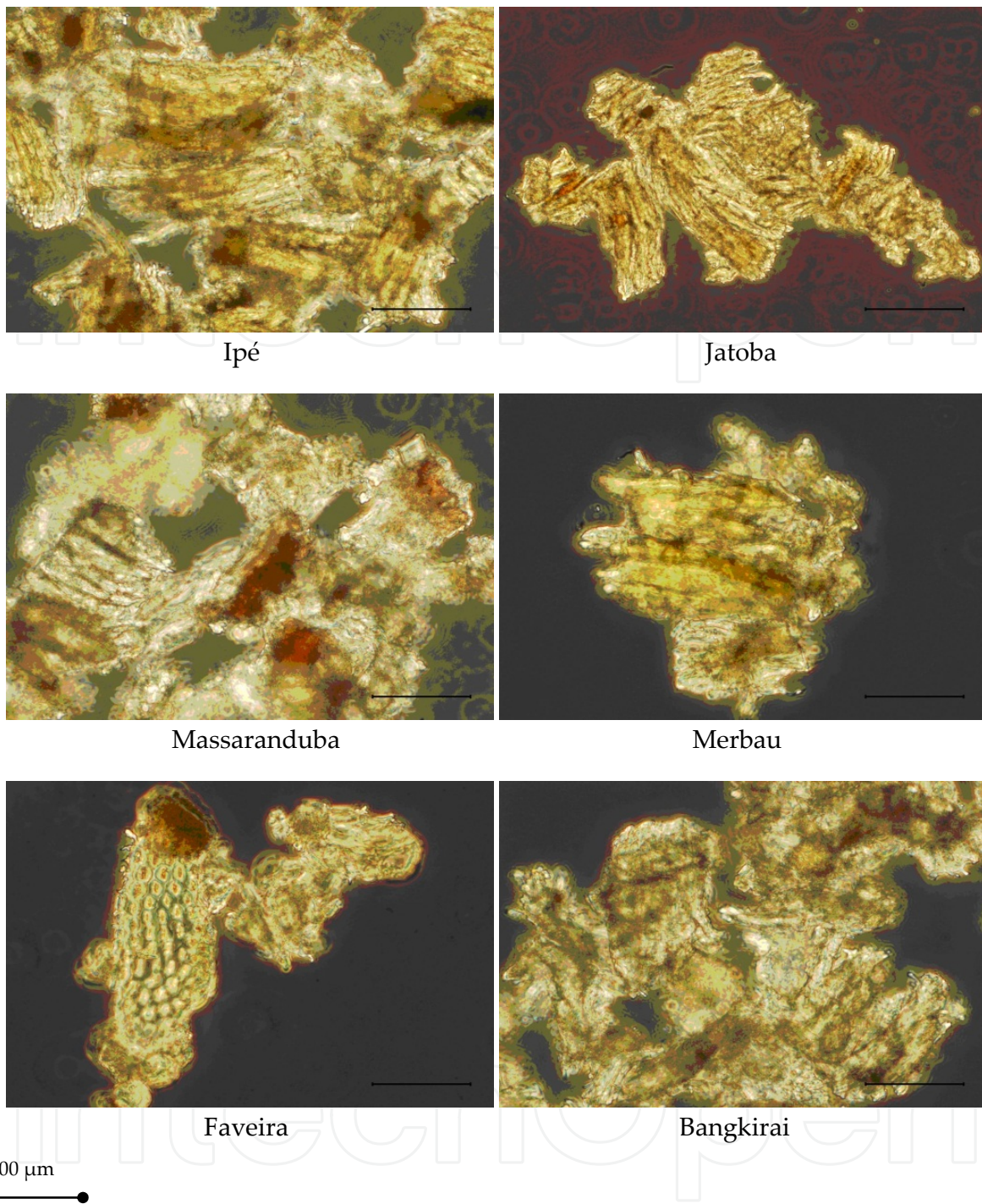


Figure 25. Microscopic pictures of sedimented dust after woods grinding

Apart from the dominant polymeric components of the woods (cellulose, hemicellulose, lignin), the woods also contain low-molecular substances. Those substances are sometimes classified as so-called extractable components, and they can be extracted from the wood material by various combinations of extraction agents.

Many of those substances, such as terpenoids, phenols, tannins, chinons, stylbens, flavonoids, alkaloids, etc., feature biological activity, both positive and negative. The

disruption of wood matter by technological operations means that one can anticipate different distributions of dominant wood components as well as low-molecular substances on the surfaces of nanoparticles (microparticles).

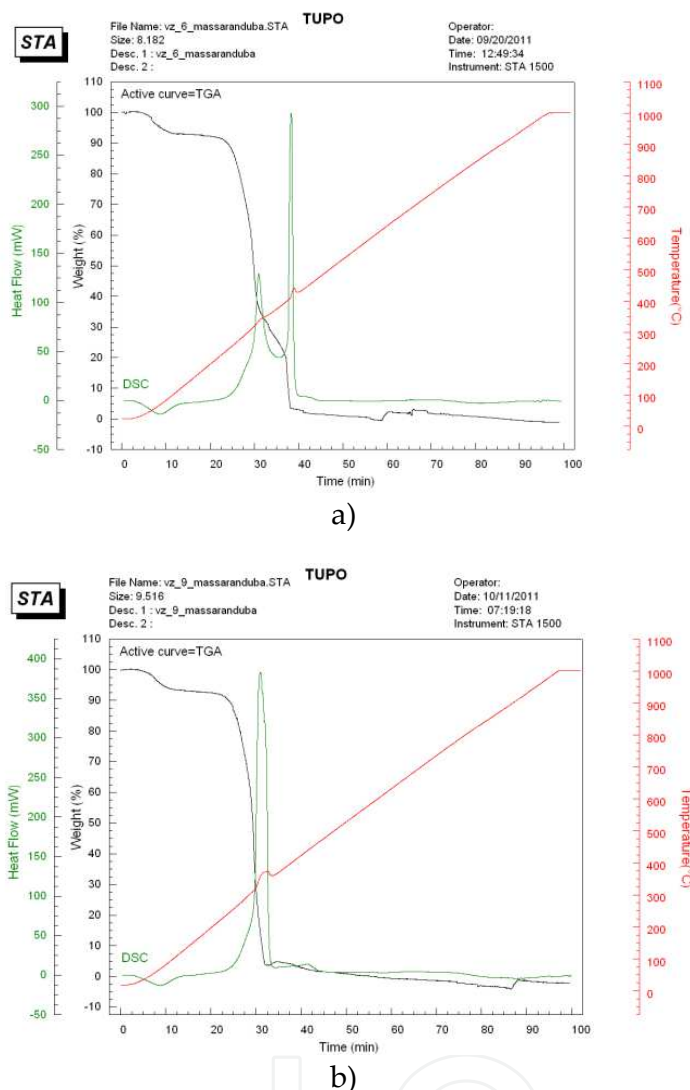
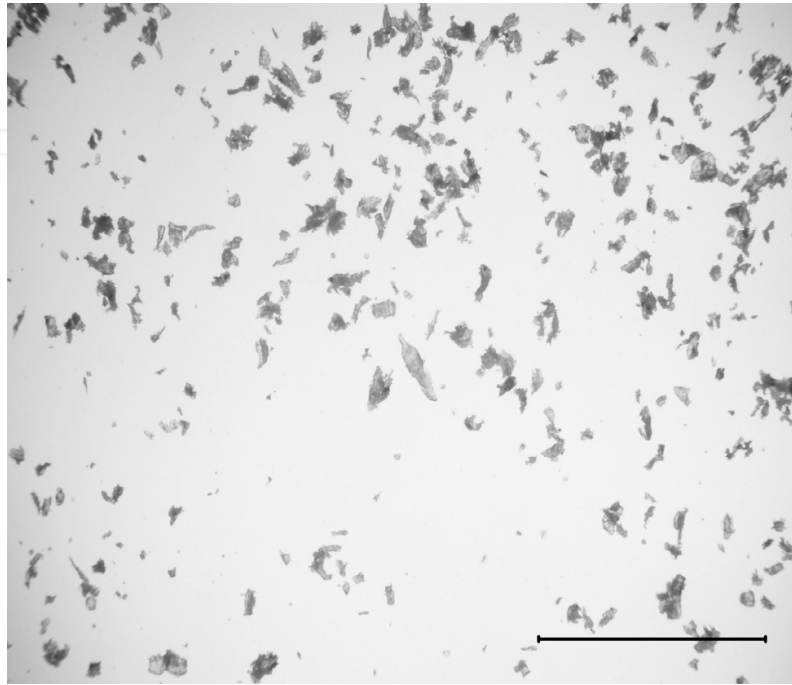


Figure 26. Thermal gravimetric analysis of sedimented dust generated with the grinding belt grain size 80 (a) and 100 (b)

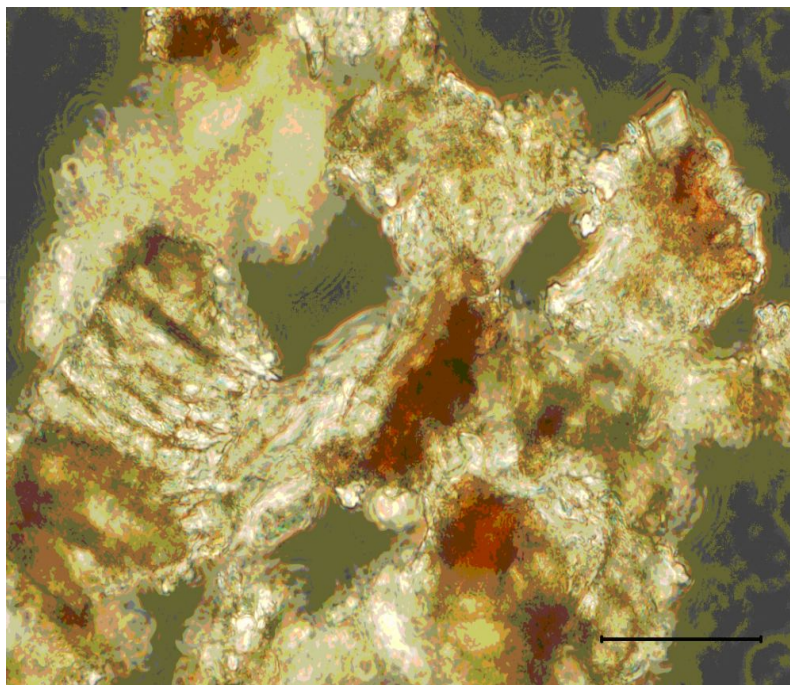
The differences in the size, shape, and certain physical properties of the particles of sedimented dust from the wood grinding have been described above. We can only speculate about the extent to which the shape of particles may influence their toxic effects. Sharp particles may behave in the organism similarly as has been described for asbestos (pulmonary fibrosis) or chronic tracheitis.

The size of the particles influences their shape, which we have illustrated with the shapes of particles generated by grinding Massaranduba and Jatoba woods. Figure 27 shows a comparison of microscopic pictures of particles with the size of hundreds of μm and particles with the size of units of μm , made by electron microscope, using particles trapped between the levels A and B in the cascade impactor.

Figure 28 shows electron microscope images of particles generated by grinding the Massaranduba wood trapped between A-C sorting levels in the cascade impactor for the Jatoba wood.



1 mm



100 μm



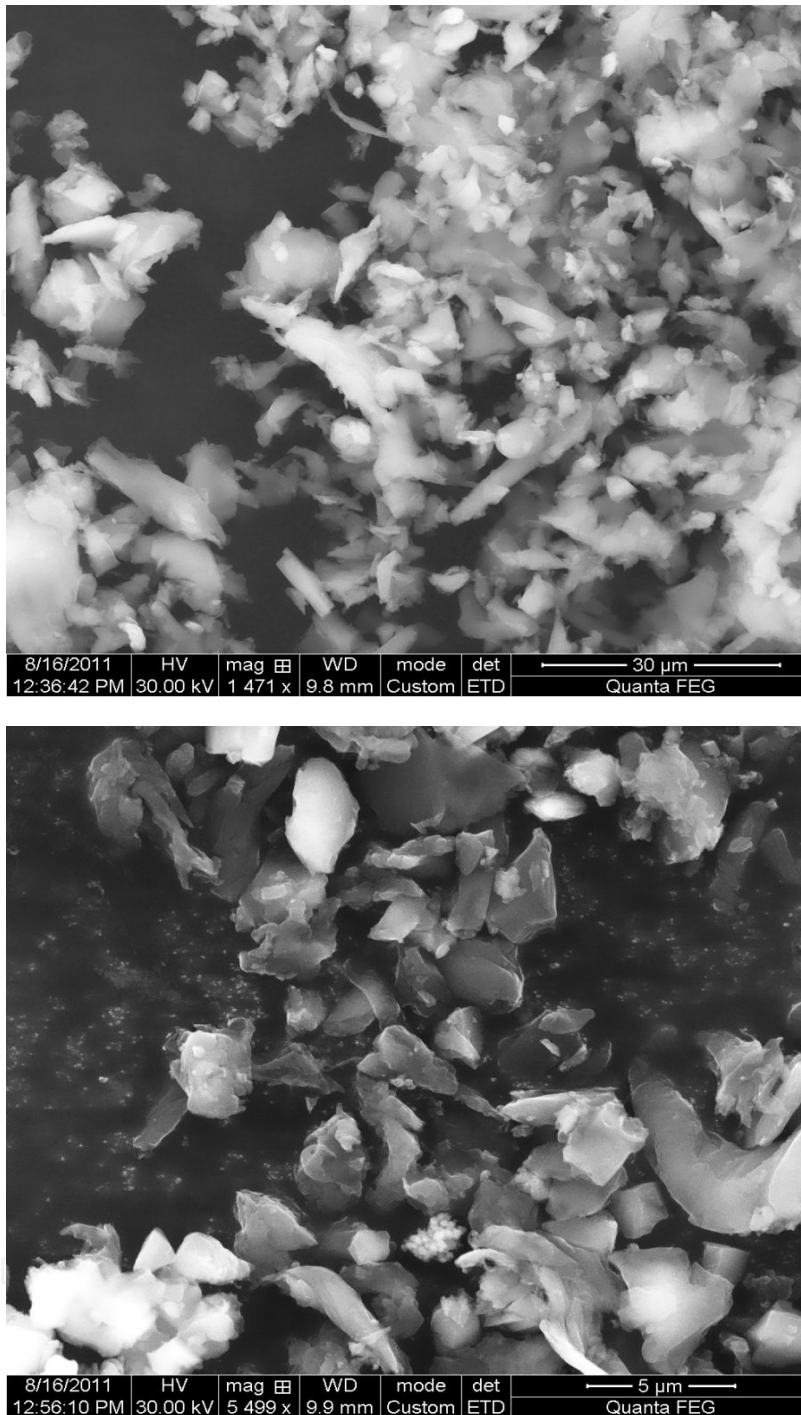
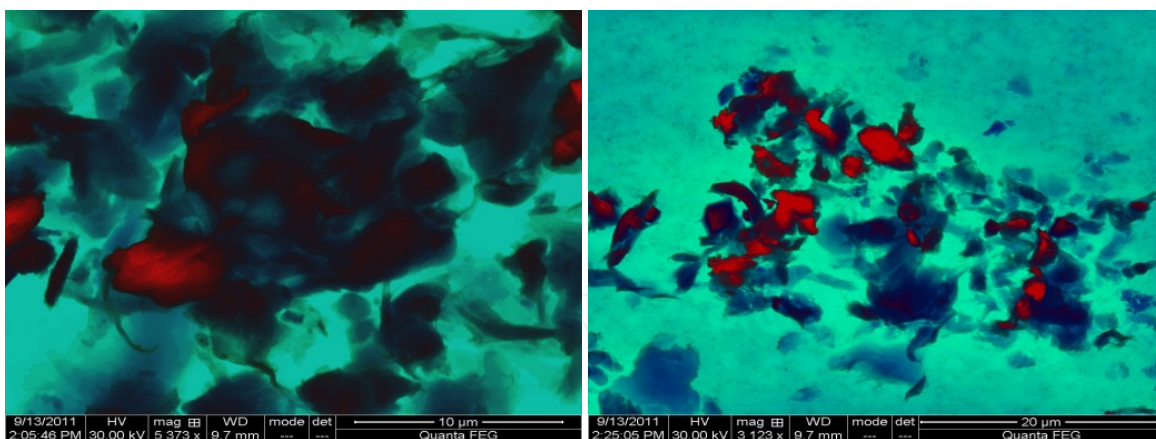


Figure 27. Comparison of the shape and size of Massaranduba wood particles

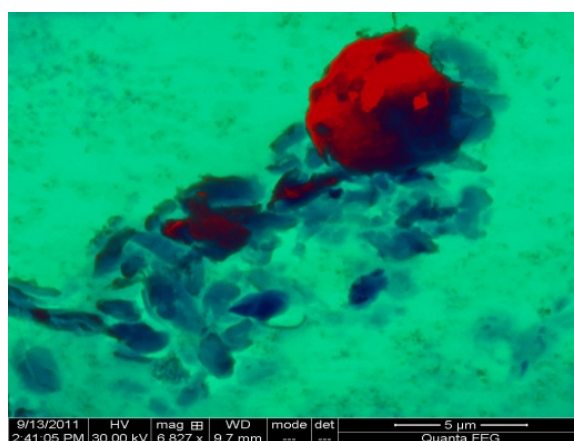
A general conclusion can be drawn that the world's major occupational health agencies only provide warnings about the risks in their reports for selected individual types of wood, and they request better protection of particular body parts (skin, eye mucosa, respiratory tract).

Our measurements have led to a recommendation that the selection of safety measures to protect the health of the employees during some technological operations with woods should take into account the character (type) of the processed wood.



Sorting level A

Sorting level B



Sorting level C

Figure 28. Electron microscope pictures of Jatoba wood particles generated by grinding.

Based on the available toxicological information about a particular wood, or based on measurements similar to those we have made for the anticipated technological operation, it will be necessary to specify or to expand the preventive measures with the objective of minimizing the contact of workers with particles generated by the processing. The measures may include technical (e.g. wetting system) and organizational measures (e.g. shorter exposure, alternation of workers), personal protective equipment (e.g. HEPA respirators: our measurements have demonstrated their 93-97% effectiveness) or health related measures (e.g. shortened intervals between medical checkups).

3.5. Measurements of quantities and distribution of aerosol nanoparticles in some steelworks operations

Metallurgic operations rank among the biggest producers of wastes of all types and categories. They include e.g. production wastes, slag, waste sludge, wastewater and emissions of heavy metals, associated with high-temperature processes of metal vapours formation and their condensation or potential chemical transformation.

Thanks to the pro-active approach of the company EVRAZ Vítkovice Steel, a.s. to the environment and safety of their employees, we were able to perform measurements of quantities and distribution of aerosols during the operation in various parts of the steelworks that utilize oxygen steelmaking.

The basis of the oxygen steelmaking (i.e. oxidation) is the removal of undesired impurities from the raw iron melt. The key elements that are converted into oxides in the process are carbon, silicon, manganese, phosphor and sulphur.

The oxygen steelmaking process is discontinuous and may be divided into the following steps:

- a. Preparation and storage of metal melt
- b. Pre-treatment of the metal melt (desulfurization of the melt by introduction of calcium carbide, magnesium and lime)
- c. Oxidation in the oxygen converter
- d. Secondary metallurgy (i.e. vacuum metallurgy)
- e. Casting (slab casting)

Before the experimental measurement, we attempted to identify locations with the expected increased emission levels, specifically:

- at the converter gas,
- during the desulfurization process,
- during handling of scraps and iron ore,
- during slag removal,
- during casting, pourover of raw iron or steel.

Meanwhile, we had to consider the safety of the workers performing the measurements and sensitivity of the employed technology to the environment in which it operates, e.g. high temperature, explosive environment, etc.

The selected locations in the premises of continual steel casting and in the converter hall of the steelworks represented the resulting compromise.

3.6. Experimental part

Measurements were conducted under regular operation of the steelworks. For safety reasons, measuring instruments to measure quantities and distribution of aerosol nanoparticles were situated only in the following locations:

- a. at the equipment for continual casting, ca. 3 m from the slab, which had been already in the horizontal position and in the area of the so-called secondary cooling, ca. 6 m from the flame-cutting machine (Figure 29).
- b. in the steelworks dispatching section, ca. 3 m from the scarfing machine, where the cooled slab was parted crosswise (Figure 30).

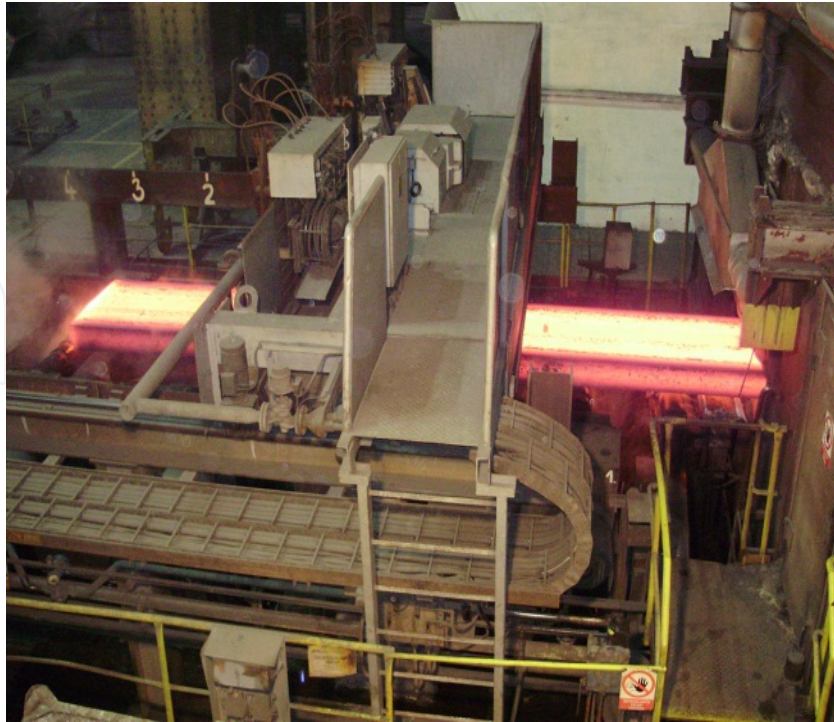


Figure 29. Measuring point at the slab continual casting



Figure 30. Measuring point in the steelworks dispatching section (at the scarfing machine)

Measurements of particles trapped in personal cascade impactors were performed in the convertor hall of the steelworks in 2 selected locations under the technological conditions described below.

3.7. Distribution of nanoparticles in the premises of the continual casting equipment

3.7.1. Measuring point a)

The average flow rate in the first location was $0.12 \text{ m}\cdot\text{s}^{-1}$ (determined with TESTO 445 with a thermal probe). 6 spectrums were measured in total with the distribution of size of aerosol particles ranging from 14 to 736 nm. The distribution of the size of aerosol particles obtained by averaging the collected spectrums is shown in the diagram in Figure 31, Table 9.

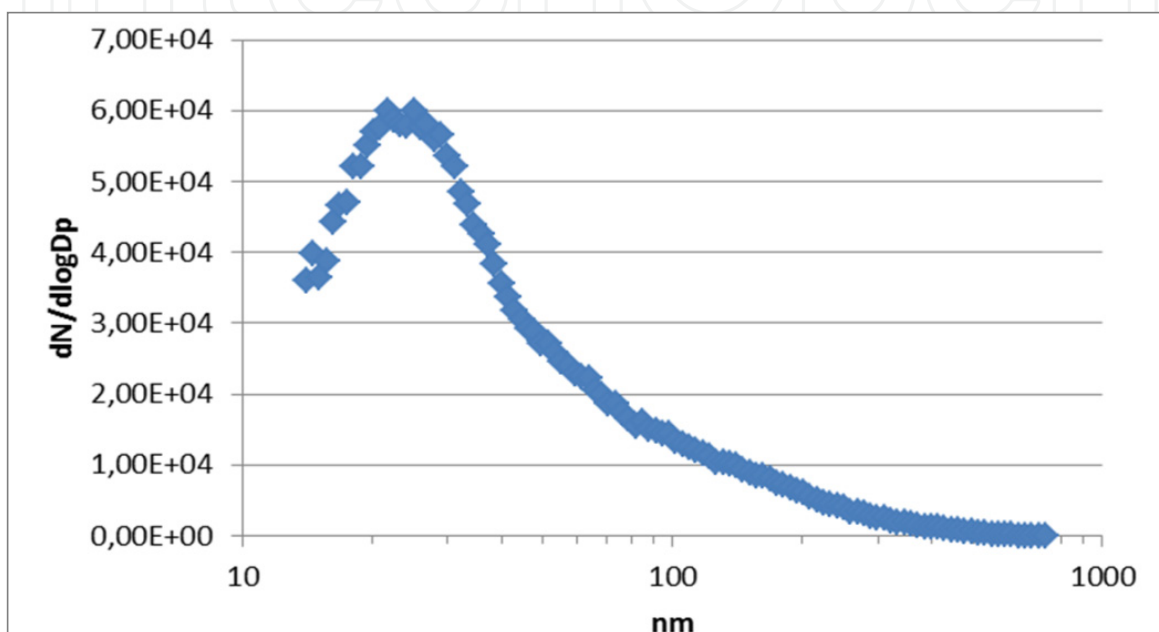


Figure 31. Distribution of aerosol particles in the measuring location a)

The mode of the collected spectrum is around 20 nm. The presented spectrums indicated presence of particles under 10 nm, which may be estimated from the size distribution

Measuring point a)	Overall concentration ($\text{N}\cdot\text{cm}^{-3}$)	Total surface of the particles ($\text{nm}^2\cdot\text{cm}^{-3}$)	Total volume of the particles ($\text{nm}^3\cdot\text{cm}^{-3}$)	Total weight of the particles ($\mu\text{g}\cdot\text{m}^{-3}$)
Average values	$3.57 \cdot 10^4$	$6.46 \cdot 10^8$	$2.33 \cdot 10^{10}$	28

Table 9. Measured physical values of nanoparticles – point a)

3.7.2. Measuring point b)

The average flow rate in the location was $0.27 \text{ m}\cdot\text{s}^{-1}$. The distribution of size of aerosol particles obtained in this measurement location is shown in the diagram in Figure 32, Table 10.

The higher flow rate has probably also affected the uneven distribution of the size of aerosol particles. The different technological development of the operation during which the measurement was performed also played a role.

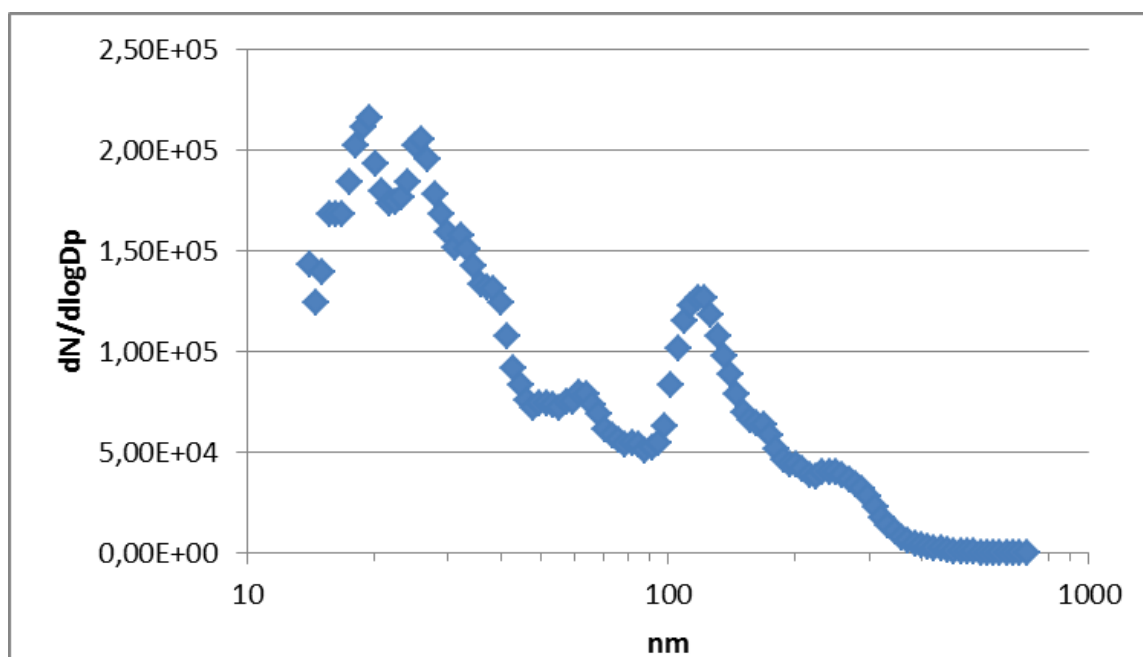


Figure 32. Distribution of aerosol particles in the measuring point b)

The maximum peak of the doublet shape in the area around 20 nm corresponds to the distribution measured in the measuring point a) but the concentration of the particles was higher. Another area with an increased number of particles is around 120 nm, while this phenomenon was not observed in the previous case. The overall concentration of particles in the nano area is by one order of magnitude higher, the weight of the particles 5x higher than in the previous case.

Measuring point b)	Overall concentration ($N \cdot cm^{-3}$)	Total surface of the particles ($nm^2 \cdot cm^{-3}$)	Total volume of the particles ($nm^3 \cdot cm^{-3}$)	Total weight of the particles ($\mu g \cdot m^{-3}$)
Average values	$1.4 \cdot 10^5$	$4.03 \cdot 10^9$	$1.38 \cdot 10^{11}$	166

Table 10. Measured physical values of nanoparticles – point b)

3.8. Measurements of the weight of trapped aerosol particles in selected locations of the steelworks convertor hall

During the performed technological operations in the steelworks convertor section, the following measuring points were selected:

- during the poulover of pre-treated raw iron into the converter after desulfurization,
- during the poulover of pre-treated raw iron from the railway carriage at the blast furnace into the ladle,

with impactors for collection of aerosol particles sorted in agreement with the specified sorting levels (Table 11). The table contains the subsequently weighed particles by fractions and conversions into volume concentrations in the proximity of the technology operation.

Sampling point	Sorting level (μm)	Trapped particles ^{a)} (mg)	Conversion into volume concentration (mg/m^3)
Pourovers into the pre-treated melt	A 2.5	0.12	2.40
	B 1.0	0.15	3.00
	C 0.5	0.09	1.80
	D 0.25	0.12	2.40
	< 0.25	0.18	3.60
	Total	0.66	13.20
Pourovers of raw iron	A 2.5	0.38	7.60
	B 1.0	0.35	7.00
	C 0.5	0.45	9.00
	D 0.25	0.33	6.60
	< 0.25	0.38	7.60
	Total	1.89	37.80

^{a)} air flow rate 10l/min. for a period of 5 minutes.

Table 11. Individual trapped fractions of aerosols in the first impactor

Samples of trapped particles at the pourovers of raw iron were submitted for electron microscope analysis. The images made by the electron microscope based on the particles trapped in the filter by sorting levels are shown in Figures 33 and 34.

Pictures made by a scanning electron microscope show visible particles from several hundreds of nanometers to ca. $5\mu\text{m}$. The evaluation of the sizes of the observed particles has made it possible to estimate that the most numerous particles were in the range from 1 to $2\mu\text{m}$. The prevailing majority of trapped particles in fine atmospheric aerosols were spherical; see Figure 33. In agreement with the generally accepted theory, particles of the size of units of micrometers are formed directly by the solidification of finely dispersed liquid aerosol of liquid iron. If the cooling rate is sufficient, round particles with some signs of crystalline structure of atoms on the surface appear instead of crystalline formations. On the contrary, if the conditions for a transition into a solid state are different, particularly in terms of the cooling rate, then fairly interesting crystalline formations can be found between the particles, as shown in Figure 34. The resulting product is actually an aggregate of very small crystals which came into immediate contact in the atmosphere.

The entire process of formation of the fine aerosol is accompanied by a chemical reaction in which melted iron particles are in a thermodynamic imbalance with oxygen from the atmosphere, and therefore an intense exothermic chemical reaction occurs on the surface of the particles which produces oxidation products of iron. The resulting formations are shown in the pictures. A chemical analysis of particles with EDS has confirmed the variable values of the Fe/O ratio. In some cases the atomic ratio Fe/O was $> 3/2$, which may be explained by the presence of non-reacted iron in the particle core.

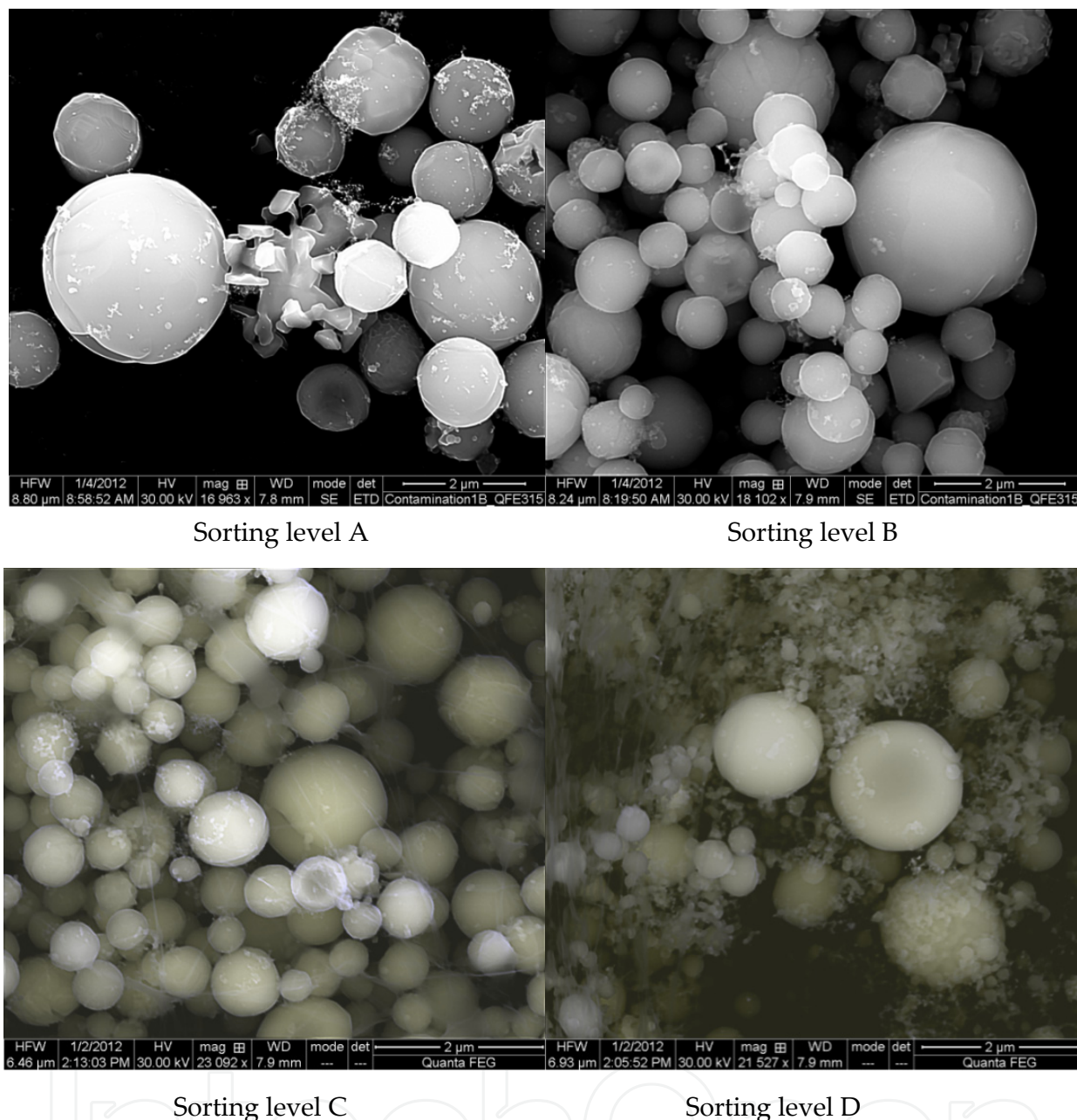
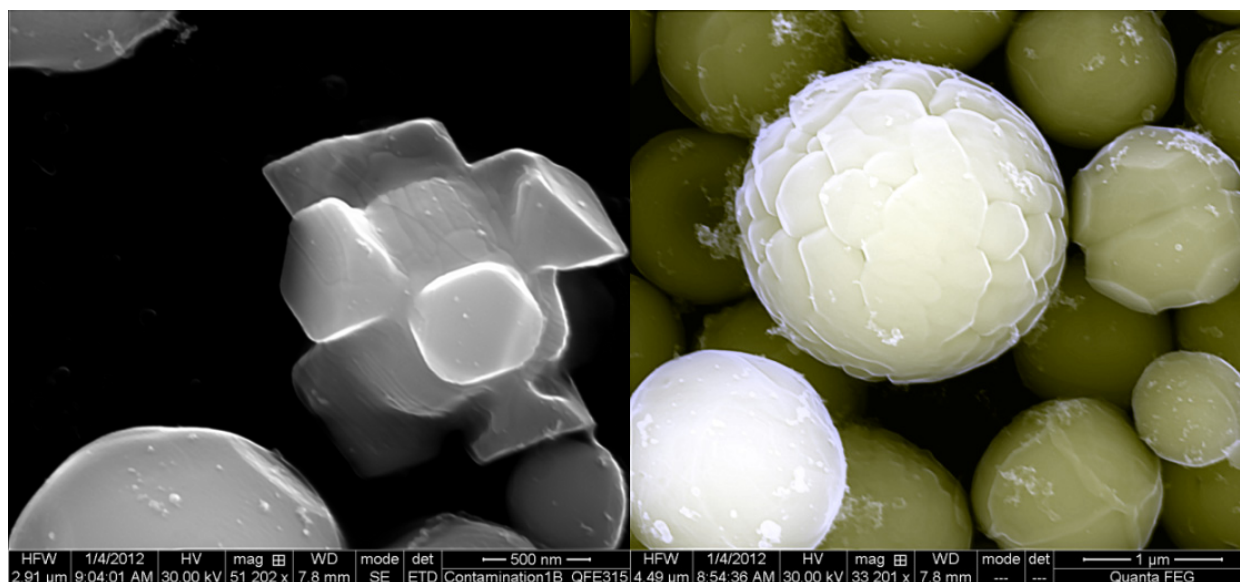


Figure 33. Images from electron microscope of nano- and microparticles from the environment of the pourover of raw iron from the railway carriage

Samples of particles trapped in the impactor were collected at the site where pre-treated melt of raw iron was poured over after desulfurization, and they were analyzed by electron microscope. In addition to the minor number of spherical particles (composed of iron, iron oxide and iron-calcium), the images also show carbon-based non-spherical and non-metallic particles. A characteristic illustration of particles trapped in the impactor is shown in Figure 35. The content of the trapped particles was probably influenced by the composition of the residual slag that remained in the melt after the tapping. The melt desulfurization, as mentioned at the beginning, is performed by the addition of calcium carbide, magnesium and lime, so the presence of calcium is completely logical.



Sorting level A

Sorting level A

Figure 34. Images from electron microscope of trapped particles of non-typical shapes from the environment of raw iron casting

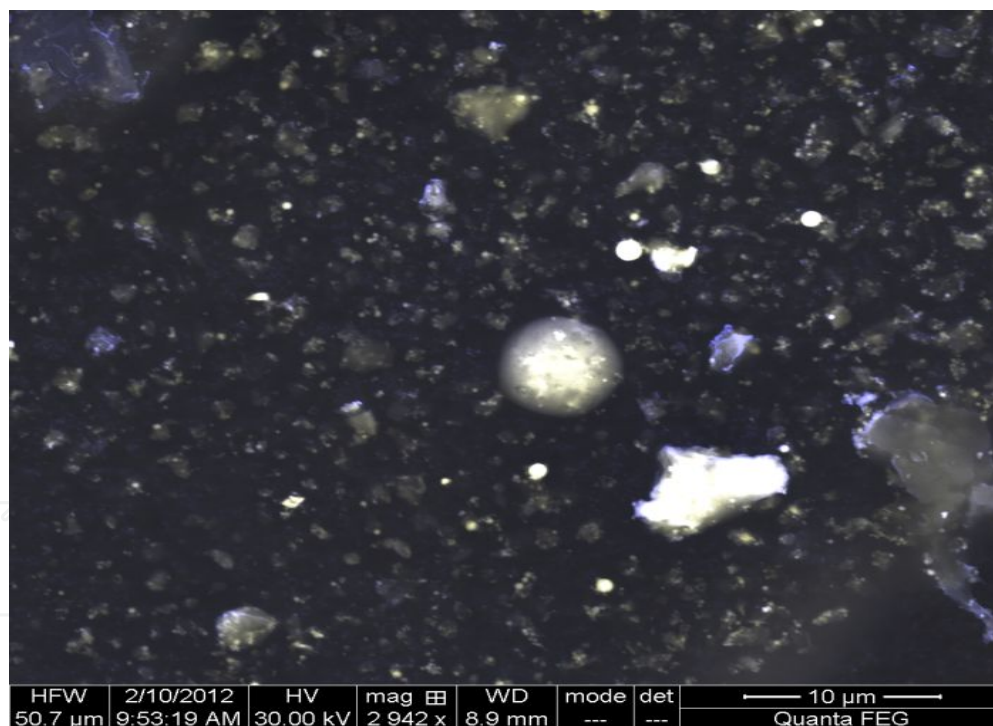


Figure 35. Electron snapshots of trapped nano- and micro-particles from the site of the pourover of pre-treated melt after desulfurization

4. Discussion about the toxicity of iron particles

Iron in suitable concentrations is an element essential for human health which participates in the transport of oxygen (hemoglobin, myoglobine) in cellular breathing. If the

concentration of iron in the organism exceeds the capacity of transport and spare proteins for iron, then it is deposited loose into the tissue. An increased deposition of iron in tissues causes fibrotization and the reduction of functional tissue. The main signs include development of liver hemosiderosis and later cirrhosis, type II diabetes, cardiomyopathy, arthritis etc. [11]

The round shape of nanoparticles probably reduces toxicity and facilitates transport from alveoli by breathing.

The concentrations of micro- and nano- particles measured in one cubic meter were higher than the permitted exposure limit (PEL) specified in the Government Order of the Czech Republic but, considering the mostly automated operation of the steelworks, the level of risk to the employees is not significant.

5. Conclusion – Examples of measures recommended based on the results of the measurements

- When designing new subway routes, the environment of the vent shaft outlets on the ground level should be taken into account
- Install effective filters into the vent shafts
- Perform consistent cleaning of the subway lining
- Replace the subway fleet (electric drives)
- Policemen should wear respirators and goggles for shooting practice
- Limit the use of entertainment pyrotechnics in residential areas
- Get as much information as possible about the origin and toxicity before processing any exotic woods
- Wear HEPA-respirators and goggles when processing exotic woods and working in the steelworks.

6. Instrumentation

The *measurements of aerosol particles* were conducted with SMPS (Scanning Mobility Particle Sizer) 3934 consisting of CPC (Condensation Particle Counter) 3022 (working in low regime) and EC (Electrostatic Classifier) 3071 equipped with DMA (Differential Mobility Analyzer), probe 3081 and impactor 0.0457 cm. The measurements were conducted using the setup scanning interval of 5 minutes, which enabled collection of samples in the range from 14 nm to 740 nm.

Aerosol particles were collected by means of a personal cascade impactor (Sioutas 225-370). The personal cascade impactor consists of four impaction levels and a filter that enables sorting and sampling airborne particles in five size intervals. Samples were collected with the personal impactor which used the sampling device QuickTake30 at a specified constant flow rate.

Micro *aerosol particles* were measured in the range from 0.5 μm to 20 μm using APS (Aerodynamic Particle Sizer Spectrometer 3321 TSI USA).

Measurements of FIT factors of the protective respirators, device PortaCount Pro+ 8038 TSI, method MAZL – 40/11 (SÚJCHBO), OSHA 29CFR1910.134.

Thermal analysis, TG-DSC and TGA were measured with the device STAi 1500 made by Instrument Specialists Incorporated - THASS

Infrared ATR spectrums (FTIR) were measured with the spectrometer Nicolet 7600 (Thermo Nicolet Instruments Co., Madison, USA) with the detector DTGS and beam divider KBr. Parameters of the measurements: number of spectrum accumulations 128, resolution 2 cm⁻¹. The measurements were conducted with an ATR cuvette Smart Orbit (Thermo Scientific) equipped with a diamond crystal.

Microscope: Microscope Olympus XI71 + CCD camera Olympus DP72 (Olympus Co., Japan) were used for magnification 200-600x.

El. microscope: made by FEI, model Quanta 450 FEG, high fiber method, ETD detector (secondary electrons) and BSE (back-scattered electrons).

Thermogravimetric and differential thermal analysis (GTA/DTA) was performed with STA; 1500 made by Instrument Specialists Incorporated – THASS.

Author details

Karel Klouda

State Office for Nuclear Safety, Czech Republic, e-mail: karel.klouda@sujb.cz

Stanislav Brádka and Petr Otáhal

The National Institute for Nuclear, Chemical and Biological Protection

7. Acknowledgement

Bílek K., Cejpek J., Dropa T., Kollárová D., Kubátová H., Matheisová H., Němeček V., Urban M., Večerková J., Vošáhlík J., Weisheitlová M., Witkovská V.

8. References

- [1] Nohavica D. (2009) Respiratory and Cardiovascular Problems Related to Nanoparticles (in Czech). Proc. of Nanocon 2009, Roznov pod Radhostem, p. 76, ISBN 978-80-87294-12-3
- [2] Klouda K., Kubátová H., Zemanová E. (2011) Nanomaterials: Prost an Contr. Communications 2/11, Vol. 13, pp. 1-13
- [3] Klouda K. (2011) Analysis of results of Measurement of Nanoparticles from Antrhopogenis Sources (in Czech). Spektrum 1/2011, pp. 19-23
- [4] Glatz A. (2010) Efficiency of Emission Particles Filters and Modern Engines Ecology are strongly Arguable (in Czech). [2010-03-16], Available: <http://biom.cz/odborne-clannky/efektivita-filtru..>

- [5] Jankovský M., Lachman J., Staszková L. (1999) Wood Chemistry (in Czech). Czech Univerzity of Life Sciences. Praha, ISBN 80-213-0559-2
- [6] Roček I. (2005) Wood of Tropical Areas (in Czech). Czech Univerzity of Life Sciences, ISBN 80-213-1346-3
- [7] Zhou G., Taylor G., Polle A. (2011) Ftir-atr-based prediction and modeling of lignin and energy contents reveals independent infra-specific variation of these traits in bio energy poplars, *Plant Methods*, 7:9, pp. 1-10
- [8] Jungnikl K., Paris O., Fratzl P., Burgert I. (2008) The implication of chemical extraction treatments on the cell wall nanostructure of soft wood, *Celulose* 15, pp. 407-418
- [9] Lau S. (1992) FT-IR spectroscopic studies on lignin from some tropical wood and rattan, *Pertanika* 14, pp. 15-81
- [10] Coates J. (2000) Interpretation of infrared spectra and practical approach. *Encyclopedia of Analytical Chemistry*, John Wiley&Sons, pp. 10815-10837
- [11] Houdak J. (2011) New information about iron metabolism in human body. Available: <http://www.slideshare.net/jirihouda/metabolismus-eleza%20/> (in Czech)